NACA RM L54H11

NACA

RESEARCH MEMORANDUM

EXPERIMENTAL INVESTIGATION AT HIGH SUBSONIC SPEEDS TO DETERMINE THE ROLLING-STABILITY DERIVATIVES OF THREE WING-FUSELAGE CONFIGURATIONS

By William C. Sleeman, Jr.

Langley Aeronautical Laboratory
Langley Field, Va.

Unclassified
Nasa Tech Pub Announcement #104
24 Nov 56

GRADE OF OFFICIAL MAKING CHANGE)

4 April 61
DATE

NATIONAL ADVISORY COMMITTEE
FOR AERONAUTICS

WASHINGTON

October 27, 1954

NATIONAL ADVISORY COMMITTEE FOR AERONAUTICS

RESEARCH MEMORANDUM

EXPERIMENTAL INVESTIGATION AT HIGH SUBSONIC SPEEDS TO DETERMINE THE ROLLING-STABILITY DERIVATIVES OF THREE WING-FUSELAGE CONFIGURATIONS

By William C. Sleeman, Jr.

SUMMARY

Rolling-stability derivatives are presented for three wing configurations, which were tested on the same fuselage, over a Mach number range from 0.50 to 0.92 and for angles of attack up to approximately 13°. These wings were assorted plan-form configurations of current interest and were not part of a geometrically related series of plan forms. Two of the wings were of aspect ratio 3 with NACA 65A004 airfoil sections parallel to the plane of symmetry and had quarter-chord sweep angles of 12.53° and 30°. An aspect-ratio-4 wing was tested which had 45° sweepback and had NACA 65A006 airfoil sections.

Even though the test wings were not related geometrically, the damping-in-roll data for the three plan forms showed similar trends with lift and Mach number in that appreciable losses in damping occurred as the lift coefficient increased from moderate to high values for the test Mach number range. Unstable damping in roll was indicated for the aspect-ratio-3 wings in the higher lift range for several Mach numbers.

The rolling derivatives through the angle-of-attack range could be estimated with good accuracy by using static-force data to account for nonpotential-flow effects for lifting conditions.

INTRODUCTION

Recent experimental results at high subsonic speeds have indicated that some wings become unstable with regard to damping in roll at moderate angles of attack (refs. 1 and 2). The present investigation was undertaken to provide information on the rolling derivatives of several

wing configurations of current interest for a Mach number range from 0.50 to 0.92 and for angles of attack up to approximately 13°.

Results obtained in the Langley high-speed 7- by 10-foot tunnel are presented for three wing configurations which were tested on the same fuselage using the forced steady-roll test technique. Two of the wings were of aspect ratio 3 with NACA 65A004 airfoil sections and had quarter-chord sweep angles of 12.53° and 30°. The other wing was an aspect-ratio-4 wing with 45° sweep and had NACA 65A006 airfoil sections.

COEFFICIENTS AND SYMBOLS

The results of this investigation are referred to the stability system of axes indicated in figure 1, which shows the positive direction of forces, moments, and velocities. Moments are referred to a center-of-gravity location on the fuselage center line and at a longitudinal position corresponding to 25-percent mean aerodynamic chord for each wing. (See fig. 2.)

A wing aspect ratio, b^2/S

b wing span, ft

C_D drag coefficient, Drag/qS

ΔC_D drag coefficient due to lift, $C_D - C_{D_{L=0}}$

$C_{D_{L=0}}$ drag coefficient at zero lift

C_L lift coefficient, Lift/qS

C_l rolling-moment coefficient, $\frac{\text{Rolling moment}}{qSb}$

C_n yawing-moment coefficient, $\frac{\text{Yawing moment}}{qSb}$

C_Y lateral-force coefficient, $\frac{\text{Lateral force}}{qS}$

$C_{l_p} = \frac{\partial C_l}{\partial(pb/2V)}$, per radian

$C_{n_p} = \frac{\partial C_n}{\partial(pb/2V)}$, per radian

$C_{Y_p} = \frac{\partial C_Y}{\partial(pb/2V)}$, per radian

$\frac{\left(C_{Y_p}/C_L\right)_M}{\left(C_{Y_p}/C_L\right)_{M=0}}, \frac{\left(C_{n_p}/C_L\right)_M}{\left(C_{n_p}/C_L\right)_{M=0}}$ Correction factors for compressibility effects obtained from reference 10

c	wing chord, ft
$\bar{c}$	mean aerodynamic chord, ft
K	induced drag factor
M	Mach number
p	rolling velocity, radians/sec
q	dynamic pressure, $\frac{\rho V^2}{2}$, lb/sq ft
pb/2V	wing-tip helix angle, radians
R	Reynolds number, based on mean aerodynamic chord
S	wing area, sq ft
V	free-stream velocity, ft/sec
α	angle of attack, deg
ρ	mass density of air, slugs/cu ft
Λ	sweep angle at quarter-chord line, deg

Subscript:

PF	potential-flow theory

MODEL AND APPARATUS

A drawing of the three wings tested and details of the fuselage used with these wings is given as figure 2. The wings which were constructed of 24S-T aluminum alloy were positioned on the fuselage center line in a manner so that the longitudinal position of the 25-percent mean aerodynamic chord point for each wing corresponded with the strain-gage balance moment center which was fixed in the fuselage. Two wings of aspect ratio 3 with NACA 65A004 airfoil sections parallel to the plane of symmetry were tested. One of these wings had a quarter-chord sweep angle of 12.53° (unswept half chord) and a taper ratio of 0.20, and the other was swept 30° with a taper ratio of 0.50. The 45° swept wing had an aspect ratio of 4, a taper ratio of 0.30, and had NACA 65A006 airfoil sections parallel to the plane of symmetry. All the wings had zero dihedral and were positioned on the fuselage with zero incidence.

The models were tested in steady roll on the forced-roll sting support shown in figure 3. Details of this test technique are given in reference 3. Various fixed angles of attack were obtained by use of offset sting adapters behind the model which were designed to allow the model to rotate about the moment reference center at each angle of attack.

TESTS AND RESULTS

Test conditions.- Tests were made in the Langley high-speed 7- by 10-foot tunnel over a Mach number range from 0.50 to 0.92 and through an angle-of-attack range from 0° to approximately 13°. The variation of mean test Reynolds number and maximum wing-tip helix angle $pb/2V$ with Mach number is shown in figure 4 for the configurations investigated.

Corrections.- Jet-boundary corrections applied to the angle of attack and drag coefficients were determined from reference 4. Blockage corrections applied to Mach number and dynamic pressure were determined from reference 5. The angles of attack of the model have also been corrected for deflection of the model and support system under load.

The support system deflected under load and these deflections combined with any initial displacement of the mass center of gravity of the model from the roll axis introduced centrifugal forces and moments when the model was rotated. Corrections for these forces and moments have been applied to the data.

Corrections for jet-boundary effects on rotary derivatives were found to be small and were not applied to the data. Corrections for wing distortion have not been applied to the data. These corrections were

negligible for the aspect-ratio-3 wings. For the aspect-ratio-4 wing, the maximum correction to C_{l_p} at zero lift was estimated to be approximately -0.02 at the highest test Mach number. This correction decreases rapidly with a decrease in damping and Mach number (ref. 3). Sting-support tares were not evaluated for the test models; however, sting tare effects for tail-off tests of other models (refs. 1 and 2) have been found negligible.

Results.- The basic results of this investigation were obtained as variations of forces and moments with wing-tip helix angle; however, since these variations were linear in most cases, only the derivatives are presented herein. Rolling derivatives of the three wing-fuselage configurations are presented in figures 5 to 7. Damping-in-roll boundaries for the test range of lift coefficient and Mach number obtained from the aforementioned derivatives and the static-force data of reference 6 is given in figure 8. Comparisons between experimental and estimated derivatives, along with some parameters pertinent to the estimations, are presented in figures 9 to 14. Estimated effects of Reynolds number at low speed are given in figures 15 and 16 for the 45° swept wing.

DISCUSSION

Basic Damping-in-Roll Results

The stability derivatives of this investigation were obtained by rotation of the model about the longitudinal stability axis and these results can be used with other derivatives with respect to the stability-axes system in the complete equations of motion in assessing airplane dynamic behavior. An airplane in free flight, however, following a rolling disturbance, would be expected to roll initially about an axis more closely alined with the principal longitudinal axis than with the stability axis. Results of the present investigation are believed to be indicative of the wing damping that would be present if the airplane was assumed to roll about the principal axis, inasmuch as the differences expected between the damping values about the stability axis and about the principal axis would be very small within the relatively low angle-of-attack range covered in the present tests.

Experimental trends of the variation of damping in roll with angle of attack for the three test wings were consistent in that, as the angle of attack was increased from 0°, the damping initially increased and then decreased at the higher angles of attack (figs. 5(a), 6(a), and 7(a)). Results for the 12.53° swept wing showed unstable regions of damping in roll at $M = 0.50$ and $M = 0.85$ (fig. 5(a)). At a Mach number of 0.70,

instability was encountered for this wing above an angle of attack of 12° and this instability was so severe that data could not be obtained for this condition.

Test results pertaining to damping in roll obtained for all the wings of this investigation are summarized in figure 8 which presents boundaries for which the damping in roll for lifting conditions is half the value at zero lift and for which the damping is zero or unstable. The dotted boundary shows the highest lift coefficient attained in the rolling tests through the Mach number range. Lines of constant altitude for level flight and an arbitrarily assumed wing loading of 100 pounds per square foot are shown to illustrate possible flight conditions, where appreciable losses in damping would be expected to occur for the wing plan forms tested.

The results in figure 8 show appreciable losses in damping for all the wings over a fairly large Mach number range. These damping losses are indicated by the presence of the dashed curves which show combinations of lift coefficient and Mach number for which the damping in roll has decreased to one-half the initial damping at zero lift. Reference to the constant-altitude lines indicates that these losses in damping would be expected to occur at reasonable operational altitudes in level flight. Although interpretation of these damping losses in terms of aircraft dynamic behavior is beyond the scope of the present paper, the desirability of avoiding conditions of neutral or negative damping in roll is apparent. Results for both the 12.53° and 30° swept wings show regions of unstable damping that would be encountered at the altitudes indicated for level flight or at lower altitudes for maneuvering conditions. Although regions of unstable damping are not indicated for the 45° swept wing within the range of lift coefficient tested, the assumption could not be made that this plan form would be satisfactory for flight conditions beyond the test limits.

Estimation of Rolling Derivatives

Rolling moment due to rolling.- A comparison of experimental and estimated C_{l_p} at zero lift is given in figure 9. Estimated results were obtained from the charts of reference 7 by using the indicated plan-form transformations to account for compressibility effects. Good overall agreement with regard to Mach number effects is shown between experiment and theory; however, values of estimated damping were somewhat lower than experiment.

Experimental and estimated damping in roll through the lift range are compared in figure 10 for the three highest test Mach numbers. The

estimated curves were determined from the relationships presented in reference 8 in which the experimental lift and drag data from reference 6 were used to account for effects of induced drag, profile drag, and variations in lift-curve slope through the angle-of-attack range.

From overall considerations, the trends with angle of attack shown by the calculated curves are in good agreement with experimental results (fig. 10); however, the reduction in estimated damping which occurred between moderate and high lift was more gradual and of smaller magnitude than was obtained experimentally. The occurrence of negative damping (positive C_{l_p}) was not indicated in the estimates (figs. 10(a) and 10(b)) but a large decrease in damping was shown for conditions where test results indicated instability.

Lateral force due to rolling.- Experimental and estimated variations of lateral force due to rolling with lift coefficient are given in figure 11 for the three test wings. Comparison of test results with estimates based on potential-flow theory (ref. 9) corrected for Mach number effects (ref. 10), where

$$C_{Y_p} = C_L \frac{A + \cos \Lambda}{A + 4 \cos \Lambda} \tan \Lambda \frac{\left(C_{Y_p}/C_L\right)_M}{\left(C_{Y_p}/C_L\right)_{M=0}} \qquad (1)$$

indicates that these estimates afford agreement with experiment near zero lift only and very large discrepancies are evident at high lift for the wings having appreciable sweep. These differences may be interpreted as an indication of the nonpotential nature of the flow over the wing for lifting conditions. A method has been developed (ref. 1) which accounts for these nonpotential-flow effects by multiplying values of C_{Y_p} obtained from equation (1) by a factor K as determined from experimental lift and drag data obtained in the usual static-force tests. Estimates based on this method show very good agreement with experimental results through the lift-coefficient range tested (fig. 11).

In reference 1, development and explanation of the method for estimating C_{n_p} and C_{Y_p} by use of an induced drag factor K was concerned primarily with the more straightforward application to C_{n_p}. Some discussion of the concepts associated with the use of this induced-drag factor with regard to C_{Y_p} might be desirable here. The factor K applied to both the aforementioned derivatives can be considered as a ratio which expresses effects of inclination of the resultant-force vector on the wing for test conditions, relative to two given flow conditions. For

assumed conditions of potential flow, the resultant-force vector would be inclined toward the wing leading edge. This inclination for a swept wing results in a lateral component of the resultant force and for rolling flight the lateral force due to roll arises from differences in this lateral-force component on the upgoing and downgoing wing panels as illustrated in the following sketch:

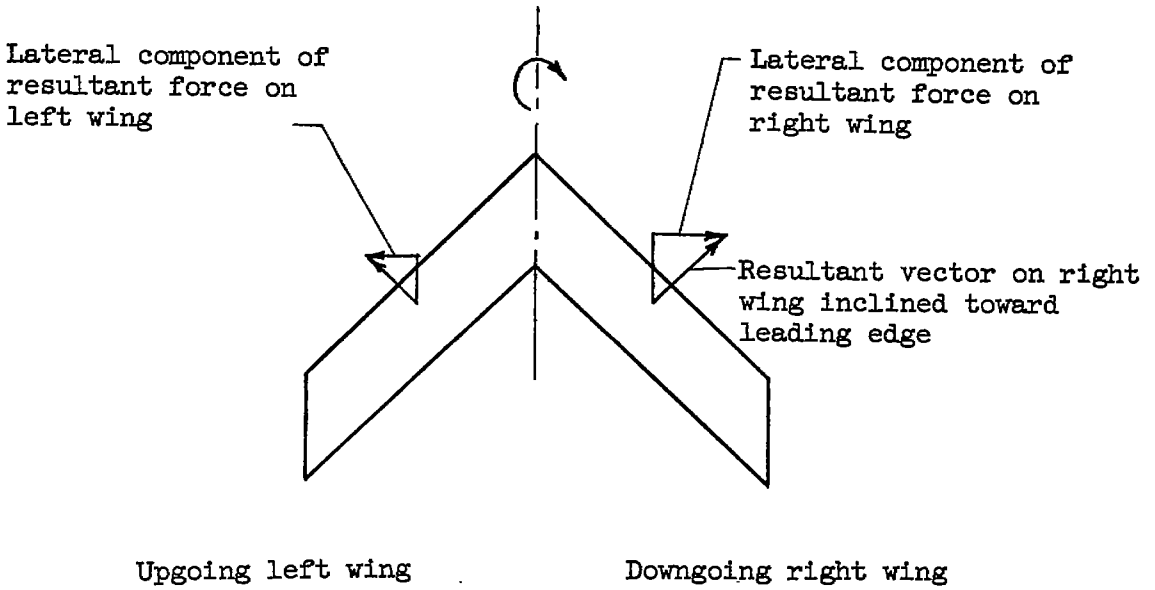

The resulting lateral force due to rolling is directed toward the downgoing wing and the value of this force is given by equation (1).

A nonpotential-flow condition which may be assumed is that for which the resultant force vector is normal to the wing surface. For this condition there would be no lateral component of the resultant force and, consequently, the lateral force due to rolling would be zero (tip suction being neglected).

Thus far the inclination of the resultant force vector has been discussed with regard to two assumed flow conditions for which values of C_{Y_p} may be readily obtained and it remains to be determined where the flow conditions encountered experimentally and the corresponding vector inclination lie relative to these two assumed conditions. The component of the resultant force parallel to the local sweep line would be expected

to be relatively invariant with angle of attack and the measured drag due to lift in the stream direction would then be proportional to the drag in the plane normal to the local sweep line. Therefore, the experimental drag results can be considered indicative of effects of inclination of the resultant force vector in that plane. Estimates of C_{Y_p} based on potential-flow theory would be expected to apply therefore if the experimental drag due to lift was in agreement with theoretical values as given by $C_L^2/\pi A$. In like manner, C_{Y_p} would be expected to be zero if the experimental drag due to lift corresponded to that given by $C_L \tan \alpha$ for the case where the resultant force is normal to the wing surface. The following expression for K is used to account for nonpotential-flow effects through the angle-of-attack range:

$$K = \frac{\frac{\partial(C_L \tan \alpha)}{\partial \alpha} - \frac{\partial(\Delta C_D)}{\partial \alpha}}{\frac{\partial(C_L \tan \alpha)}{\partial \alpha} - \frac{\partial(C_L^2/\pi A)}{\partial \alpha}}$$

Inspection of this expression indicates that, when the variation of experimental drag with angle of attack is equal to the variaton of $C_L \tan \alpha$, K is zero and no lateral force due to rolling would be expected. A value of unity for K would indicate that the experimental flow condition encountered corresponded to that for potential flow.

Experimental drag due to lift for the three test wings is presented in figure 12 and values of K determined from these results are given in figure 13 for two Mach numbers. The variation of K with angle of attack shows similar trends for the three wings, and the values of K decrease in going from low to moderate angles of attack, as would be expected. Values of K at the lowest angles, however, do not approach unity as might be expected but, in some cases, appear to approach zero. This variation at low angles is believed to be associated with Reynolds number effects on drag due to lift and will be discussed later.

Yawing moment due to rolling.- A comparison of experimental and estimated yawing moment due to rolling is presented in figure 14. Estimates based on potential-flow theory (ref. 7) corrected for compressibility effects (ref. 10) agree fairly well with experiment at low lift; however, appreciable departures are evident at moderate lift coefficients. Estimates based on the method of reference 1, where

$$C_{n_p} = -C_{l_p} \tan \alpha - K \left[-C_{l_p} \tan \alpha - C_L \left(\frac{C_{n_p}}{C_L} \right)_{PF} \frac{\left(C_{n_p}/C_L \right)_M}{\left(C_{n_p}/C_L \right)_{M=0}} \right] \qquad (2)$$

were generally in very good agreement with test results through the lift-coefficient range. Some of the discrepancies shown between experiment and estimates by using the method of reference 1 are attributable to differences in estimated and test values for damping in roll at high angles.

Estimated Effects of Reynolds Number

Experience in estimating rolling-stability derivatives for a number of wing plan forms having considerable differences in geometry and for Mach numbers up to 0.92 has indicated that these derivatives can be predicted with reasonable accuracy by using experimental static-force data to account for nonpotential-flow effects. It would, therefore, be desirable to use these estimation procedures to assess effects which could not be determined experimentally with existing equipment. One problem of interest which has not been investigated experimentally is that of the effects of Reynolds number on rolling-stability derivatives for a large Reynolds number range. Static-force data from which these effects can be estimated at low speed are presented in reference 11 for several wings of aspect ratio 4, one of which corresponds to the 45° swept wing of the present tests. Significant Reynolds number effects were indicated on drag due to lift for this wing particularly at low angles of attack and the effects might be expected to persist in the rolling derivatives.

Values of the factor K were determined for Reynolds numbers of approximately 3.0×10^6, 6.0×10^6, and 12.0×10^6 and these results are given in figure 15. Results at the lowest Reynolds number show decreasing values of K as the lift coefficient decreases from about 0.2; whereas values for the highest Reynolds number approach unity at very low lift coefficients. These results indicate that flow conditions closely corresponding to potential flow would be expected only at high Reynolds numbers and low lift for this wing; whereas, at high angles of attack, values of K were not appreciably affected by Reynolds number because the flow was separated.

Effects of Reynolds number on the rolling derivatives for the 45° swept wing are presented in figure 16 and show trends that would be expected from the preceding discussion of K. Estimates at the highest Reynolds number for all the rolling derivatives are in good agreement with potential-flow theory up to a lift coefficient of 0.2 whereas results

at $R = 3.0 \times 10^6$ for C_{n_p} and C_{Y_p} were not in agreement with potential-flow theory. At high lift, Reynolds number effects on C_{n_p} and C_{Y_p} appear negligible and effects on C_{l_p} are, to the first order, the effects of Reynolds number on lift-curve slope at high angles of attack.

CONCLUDING REMARKS

The results of an investigation to determine the rolling stability derivatives of three wing-fuselage configurations having aspect-ratio-3 wings of 12.53° and 30° sweep and an aspect-ratio-4 wing having 45° sweep indicated similar trends with lift coefficient and Mach number for an angle-of-attack range from 0° to 13° and Mach numbers from 0.5 to 0.92. Appreciable losses in damping occurred for all the test wings at high lift, and the aspect-ratio-3 wings became unstable at Mach numbers near 0.85.

Estimations of the rolling derivatives for the three geometrically unrelated wings were in good agreement with experimental derivatives when static-force data were used to account for nonpotential-flow effects for lifting conditions.

Langley Aeronautical Laboratory,
National Advisory Committee for Aeronautics,
Langley Field, Va., July 26, 1954.

REFERENCES

1. Wiggins, James W.: Wind-Tunnel Investigation of Effect of Sweep on Rolling Derivatives at Angles of Attack Up to 13° and at High Subsonic Mach Numbers, Including a Semiempirical Method of Estimating the Rolling Derivatives. NACA RM L54C26, 1954.

2. Wiggins, James W.: Wind-Tunnel Investigation at High Subsonic Speeds To Determine the Rolling Derivatives of Two Wing-Fuselage Combinations Having Triangular Wings, Including a Semiempirical Method of Estimating the Rolling Derivatives. NACA RM L53L18a, 1954.

3. Kuhn, Richard E., and Wiggins, James W.: Wind-Tunnel Investigation To Determine the Aerodynamic Characteristics in Steady Roll of a Model at High Subsonic Speeds. NACA RM L52K24, 1953.

4. Gillis, Clarence L., Polhamus, Edward C., and Gray, Joseph L., Jr.: Charts for Determining Jet-Boundary Corrections for Complete Models in 7- by 10-Foot Closed Rectangular Wind Tunnels. NACA WR L-123, 1945. (Formerly NACA ARR L5G31.)

5. Hensel, Rudolph W.: Rectangular-Wind-Tunnel Blocking Corrections Using the Velocity-Ratio Method. NACA TN 2372, 1951.

6. Goodson, Kenneth W., and Becht, Robert E.: Wind-Tunnel Investigation at High Subsonic Speeds of the Static Longitudinal Stability Characteristics of a Complete Model Having Cropped-Delta, Swept, and Unswept Wings and Several Horizontal-Tail Heights. NACA RM L54H12, 1954.

7. Bird, John D.: Some Theoretical Low-Speed Span Loading Characteristics of Swept Wings in Roll and Sideslip. NACA Rep. 969, 1950. (Supersedes NACA TN 1839.)

8. Goodman, Alex, and Adair, Glenn H.: Estimation of the Damping in Roll of Wings Through the Normal Flight Range of Lift Coefficient. NACA TN 1924, 1949.

9. Toll, Thomas A., and Queijo, M. J.: Approximate Relations and Charts for Low-Speed Stability Derivatives of Swept Wings. NACA TN 1581, 1948.

10. Fisher, Lewis R.: Approximate Corrections for the Effects of Compressibility on the Subsonic Stability Derivatives of Swept Wings. NACA TN 1854, 1949.

11. Cahill, Jones F., and Gottlieb, Stanley M.: Low-Speed Aerodynamic Characteristics of a Series of Swept Wings Having NACA 65A006 Airfoil Sections (Revised). NACA RM L50F16, 1950.

[redacted]

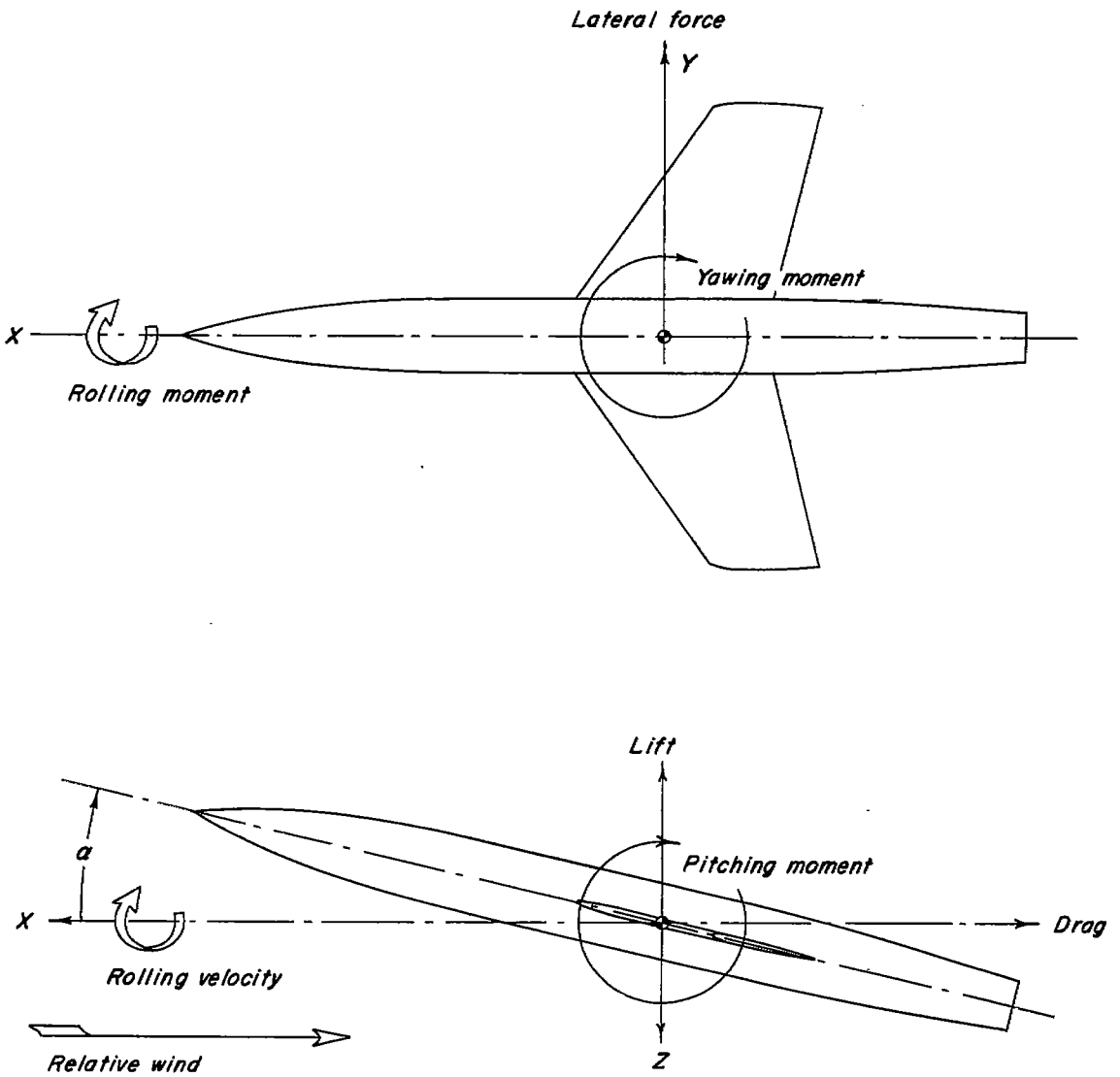

Figure 1.- System of axes used showing positive directions of forces, moments, angles, and velocities.

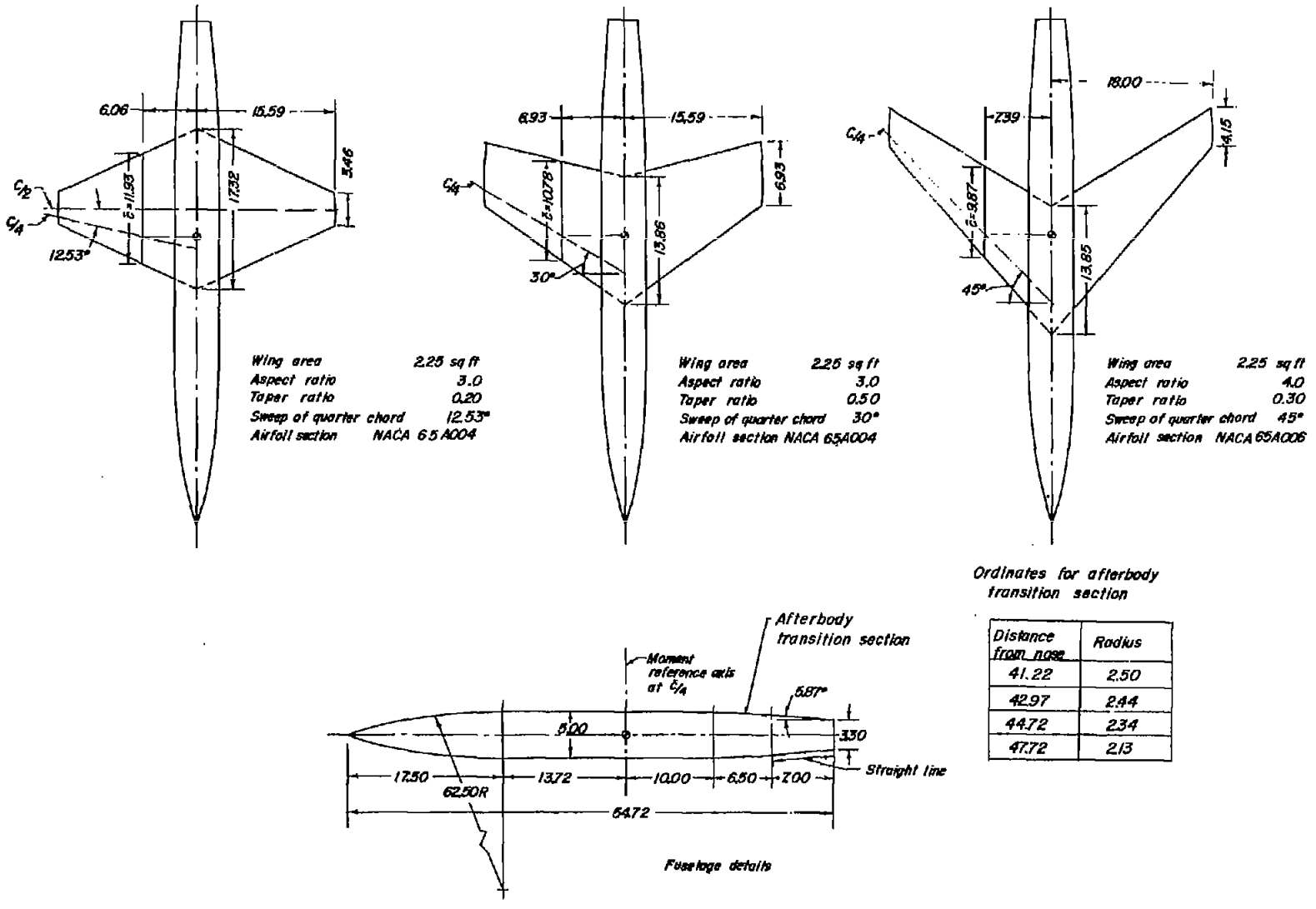

Figure 2.- Plan form of the test configurations. Dimensions are in inches unless otherwise specified.

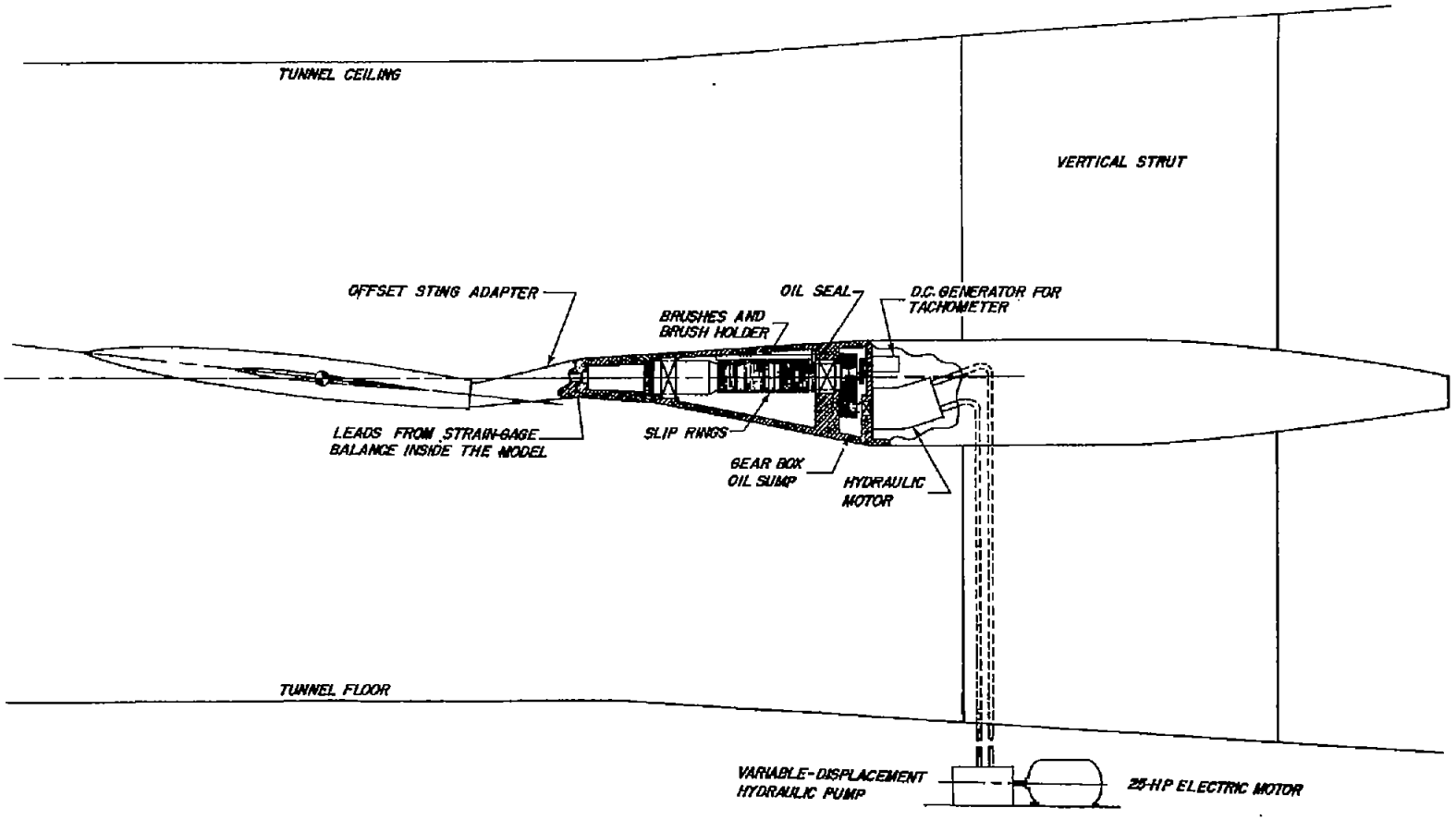

Figure 3.- General arrangement of forced-roll support system.

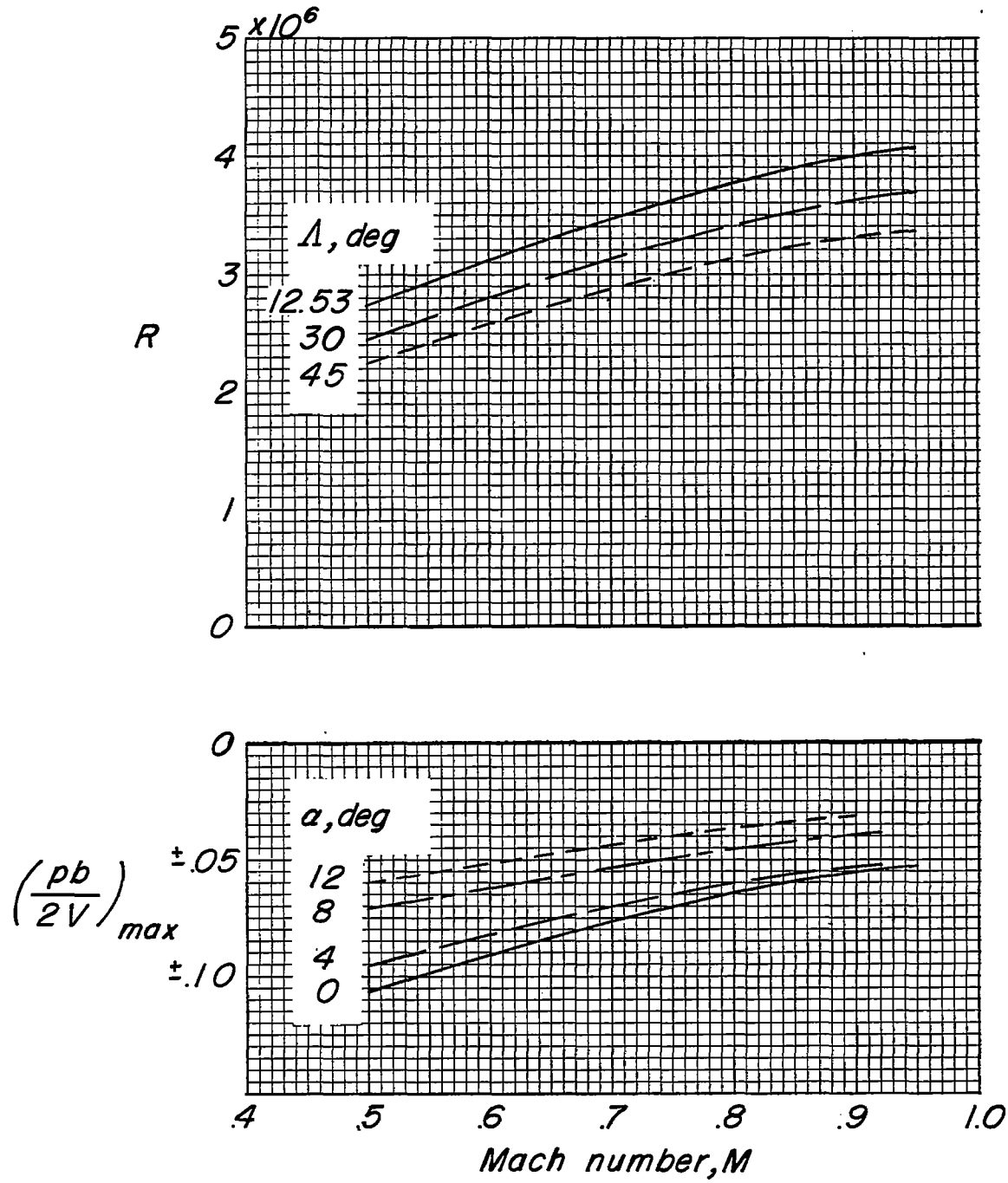

Figure 4.- Variation of test Reynolds number and maximum test pb/2V with Mach number for the three test wings.

[redacted]

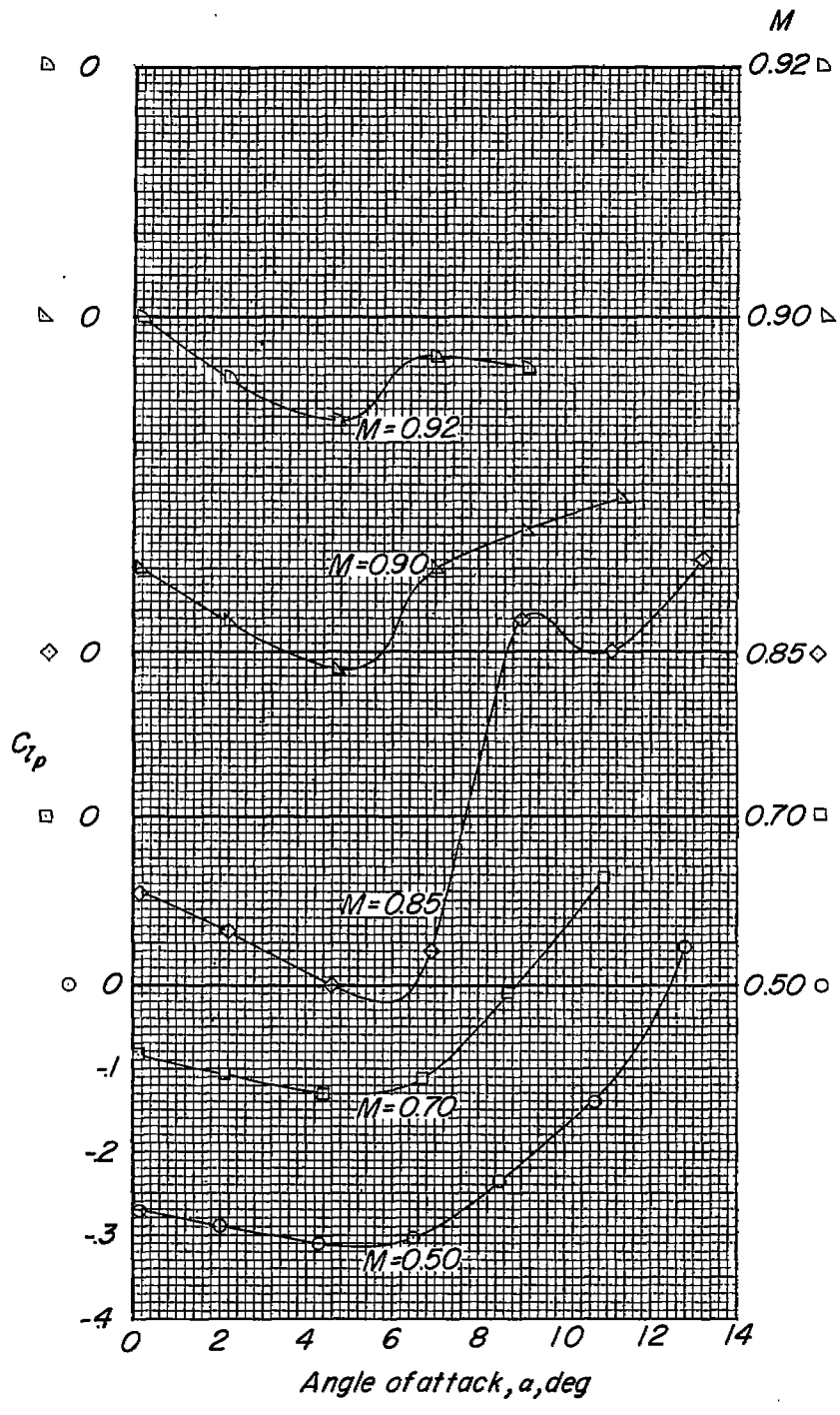

(a) Damping in roll C_{l_p}.

Figure 5.- Variation of rolling-stability derivatives with angle of attack for the aspect-ratio-3 wing swept back 12.53°.

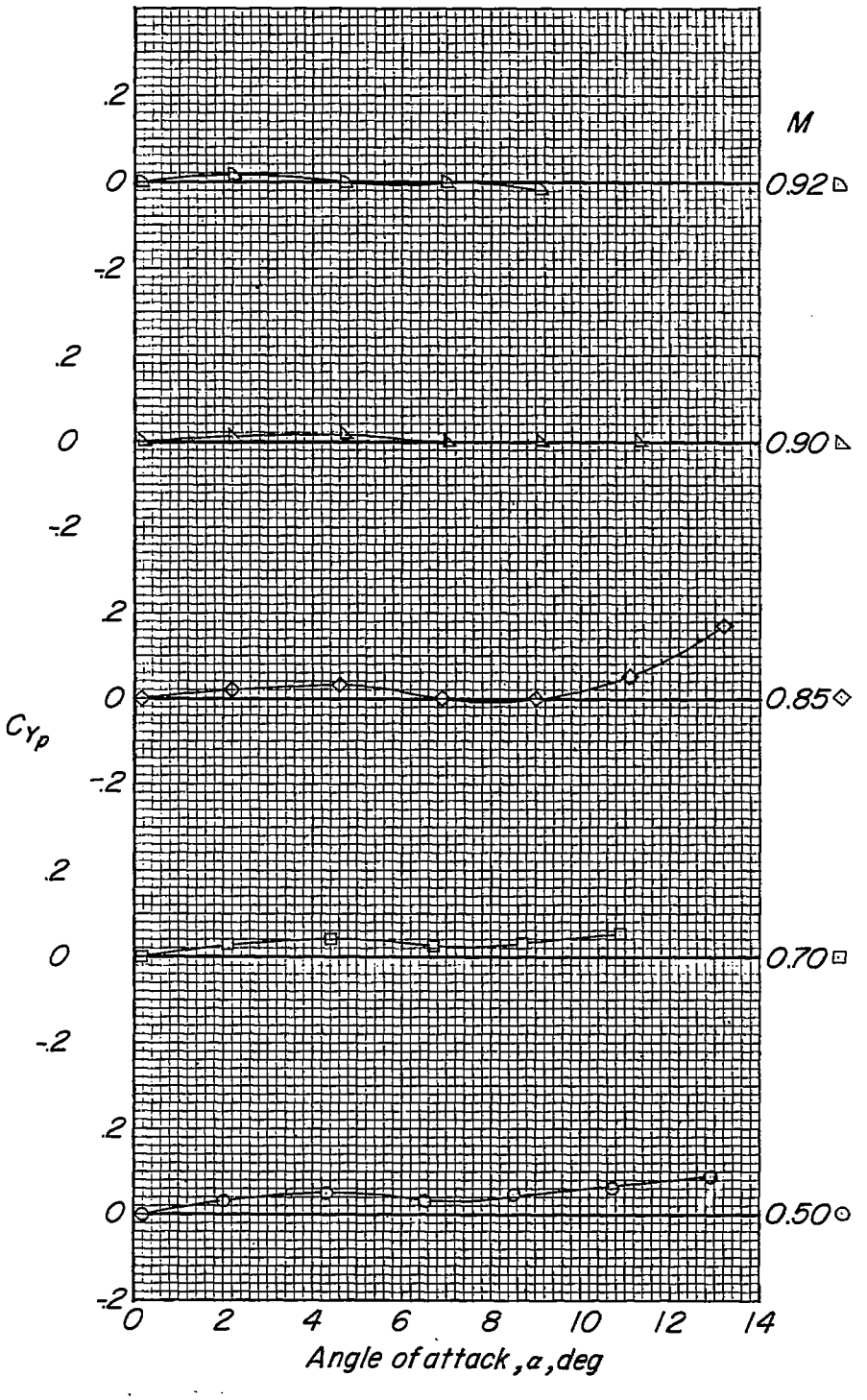

(b) Lateral force due to rolling C_{Y_p}.

Figure 5.- Continued.

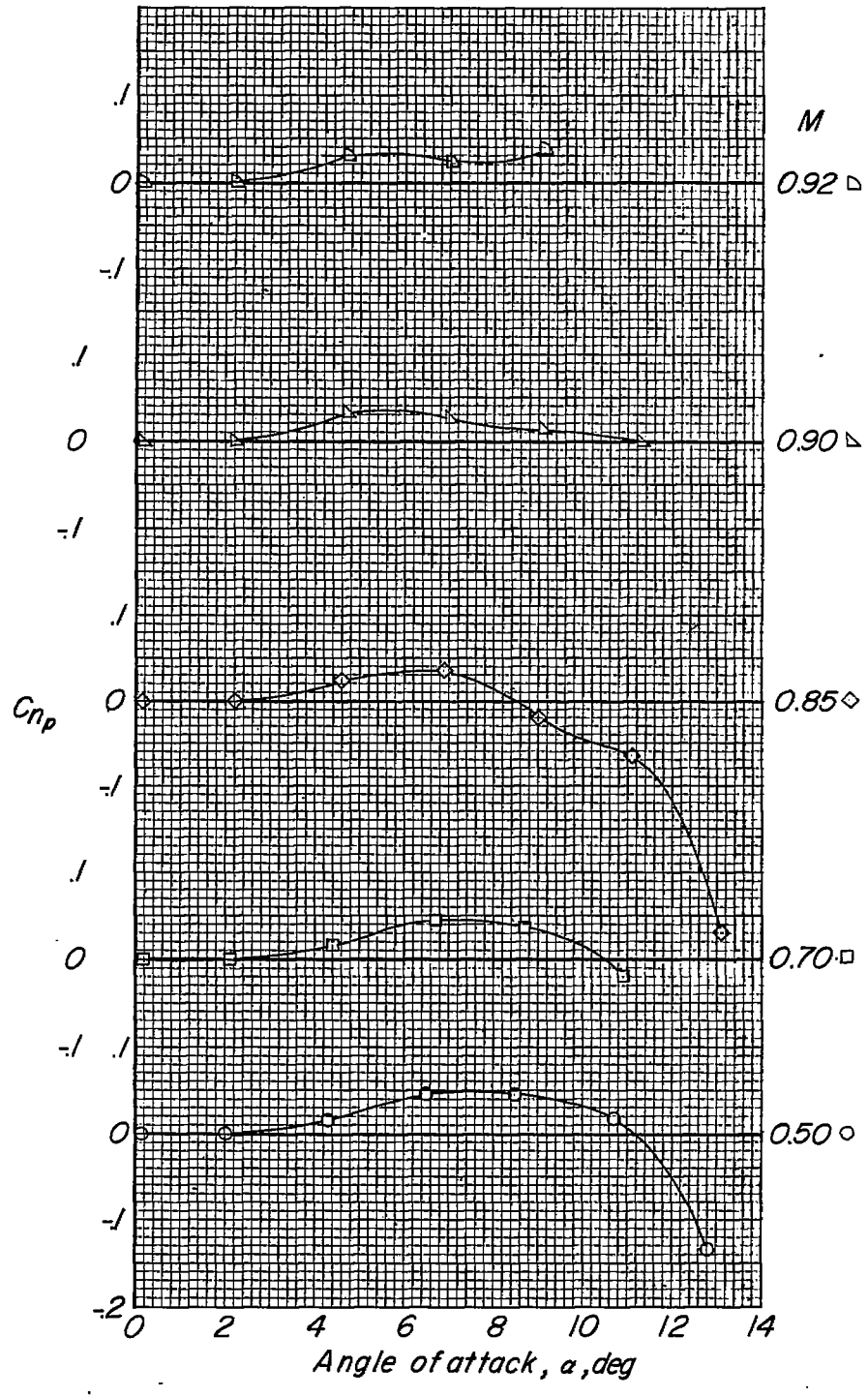

(c) Yawing moment due to rolling C_{n_p}.

Figure 5.- Concluded.

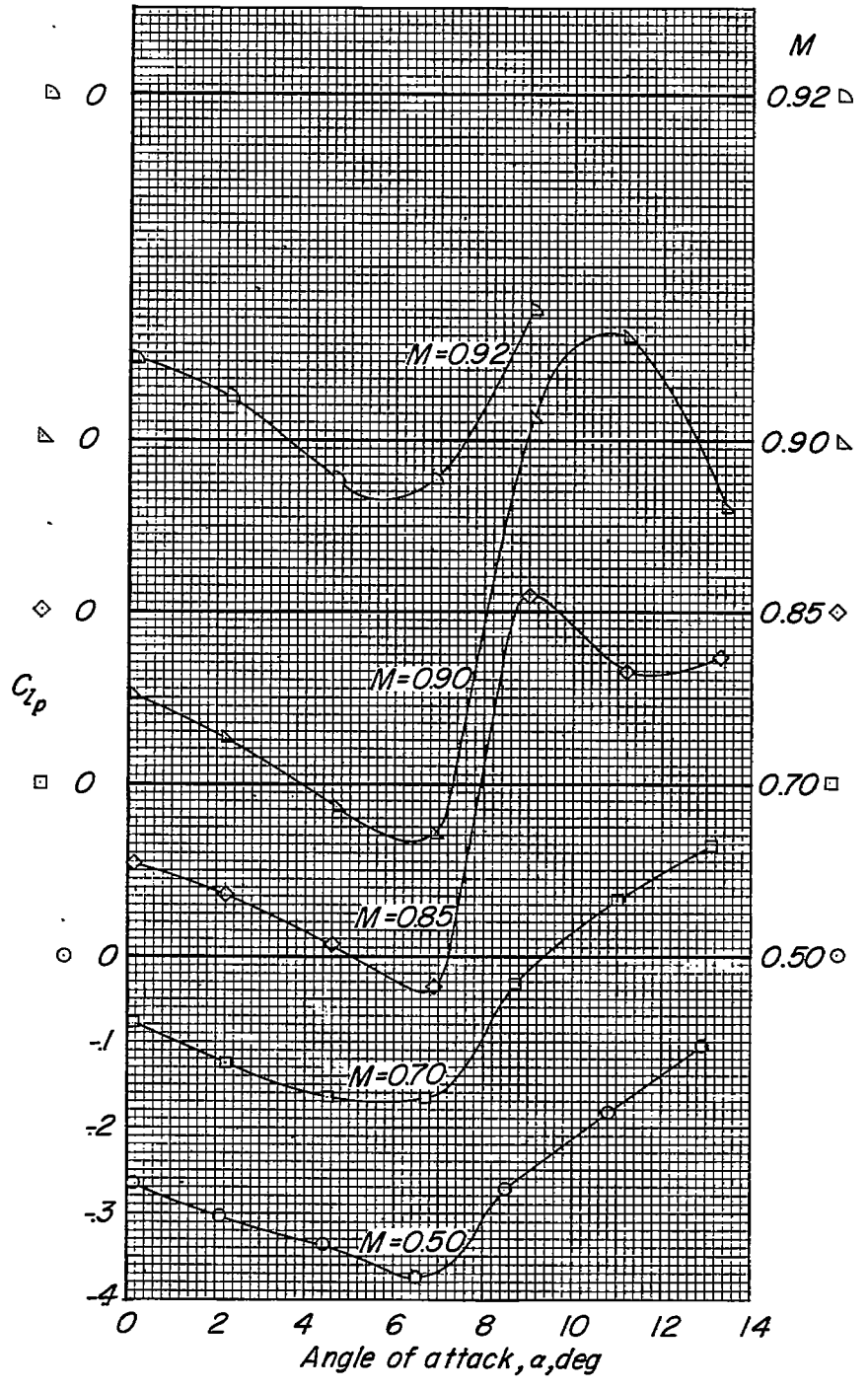

(a) Damping in roll C_{l_p}.

Figure 6.- Variation of rolling stability derivatives with angle of attack for the aspect-ratio-3 wing swept back 30°.

[redacted]

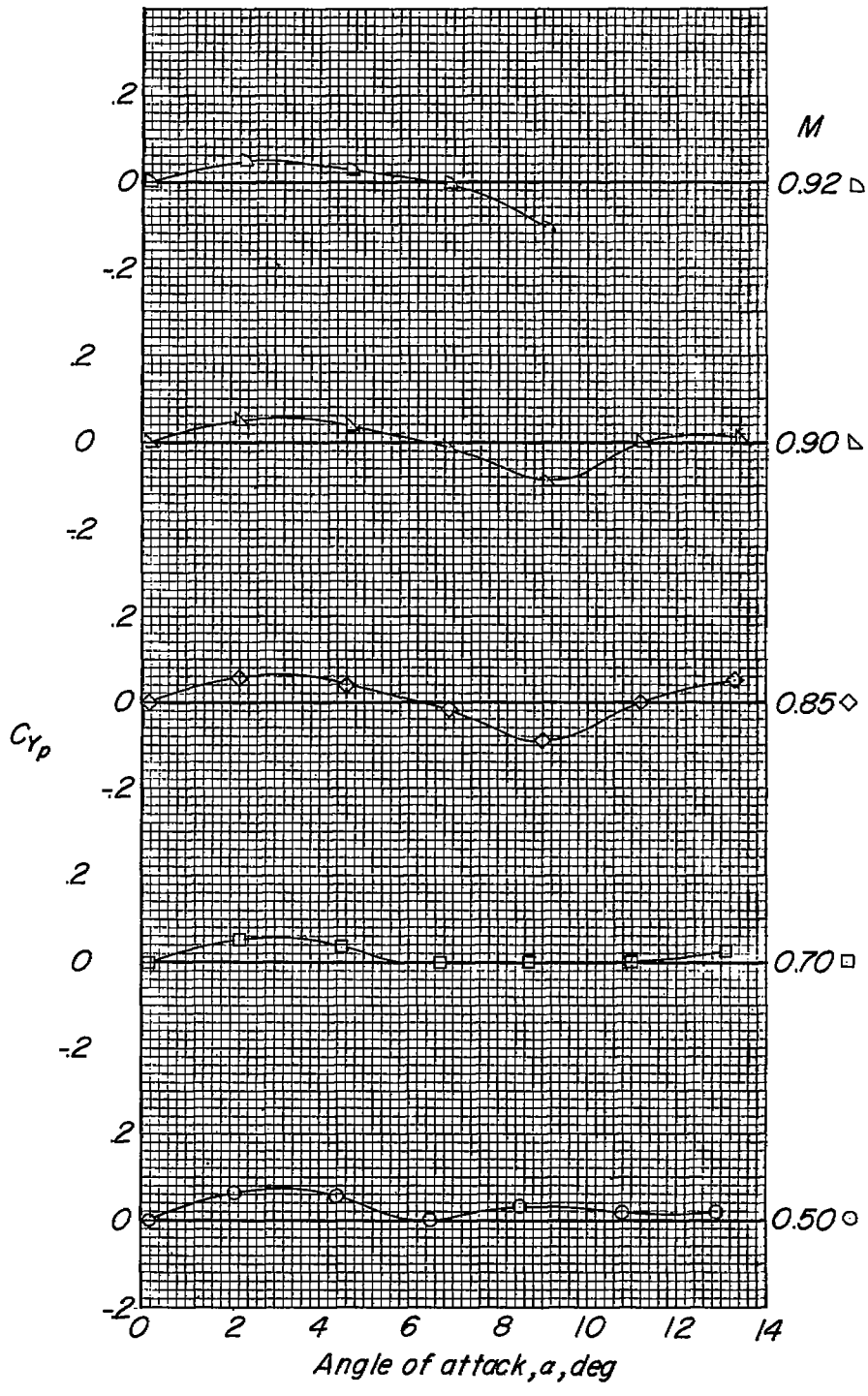

(b) Lateral force due to rolling C_{Y_p}.

Figure 6.- Continued.

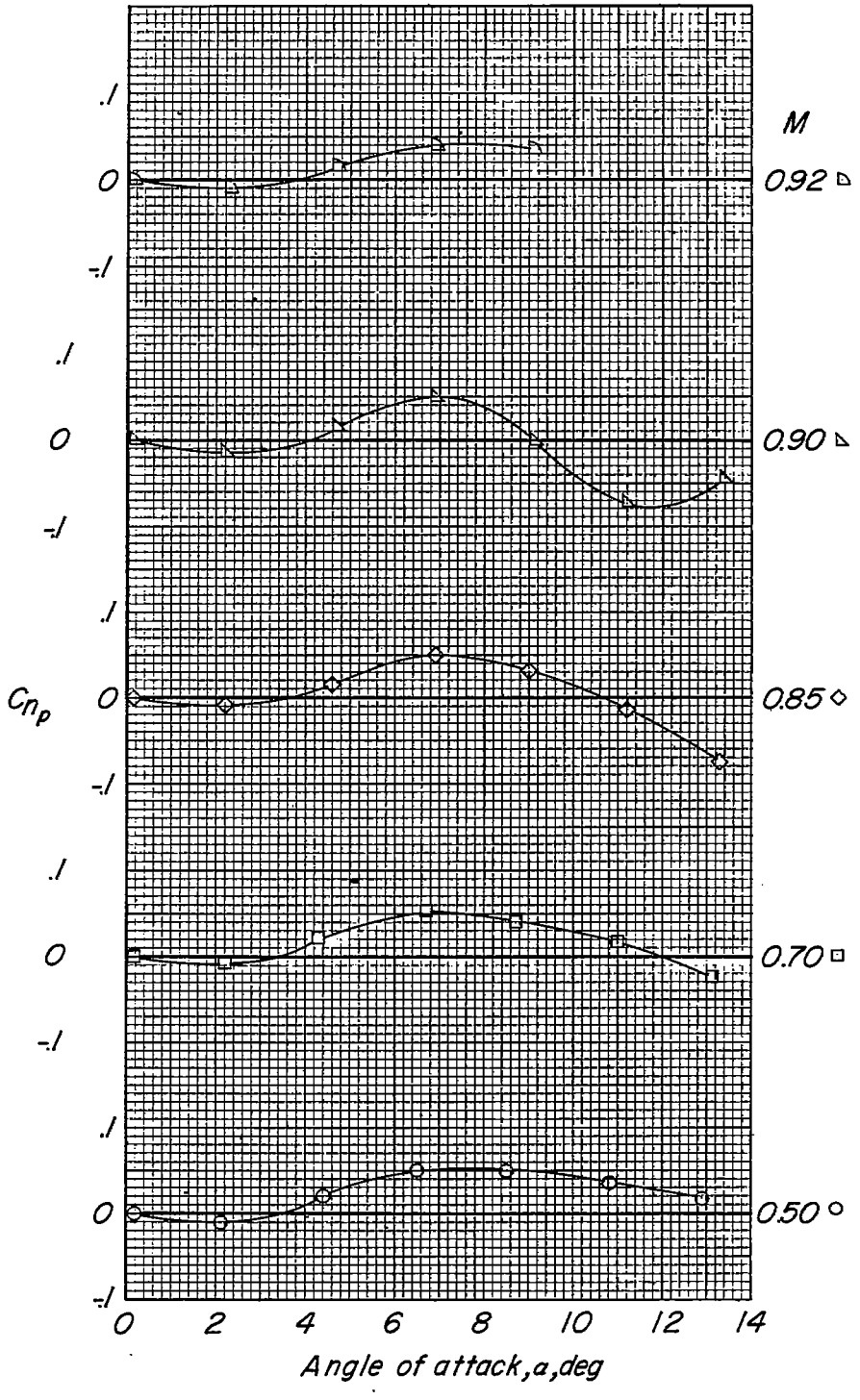

(c) Yawing moment due to rolling C_{n_p}.

Figure 6.- Concluded.

[redacted]

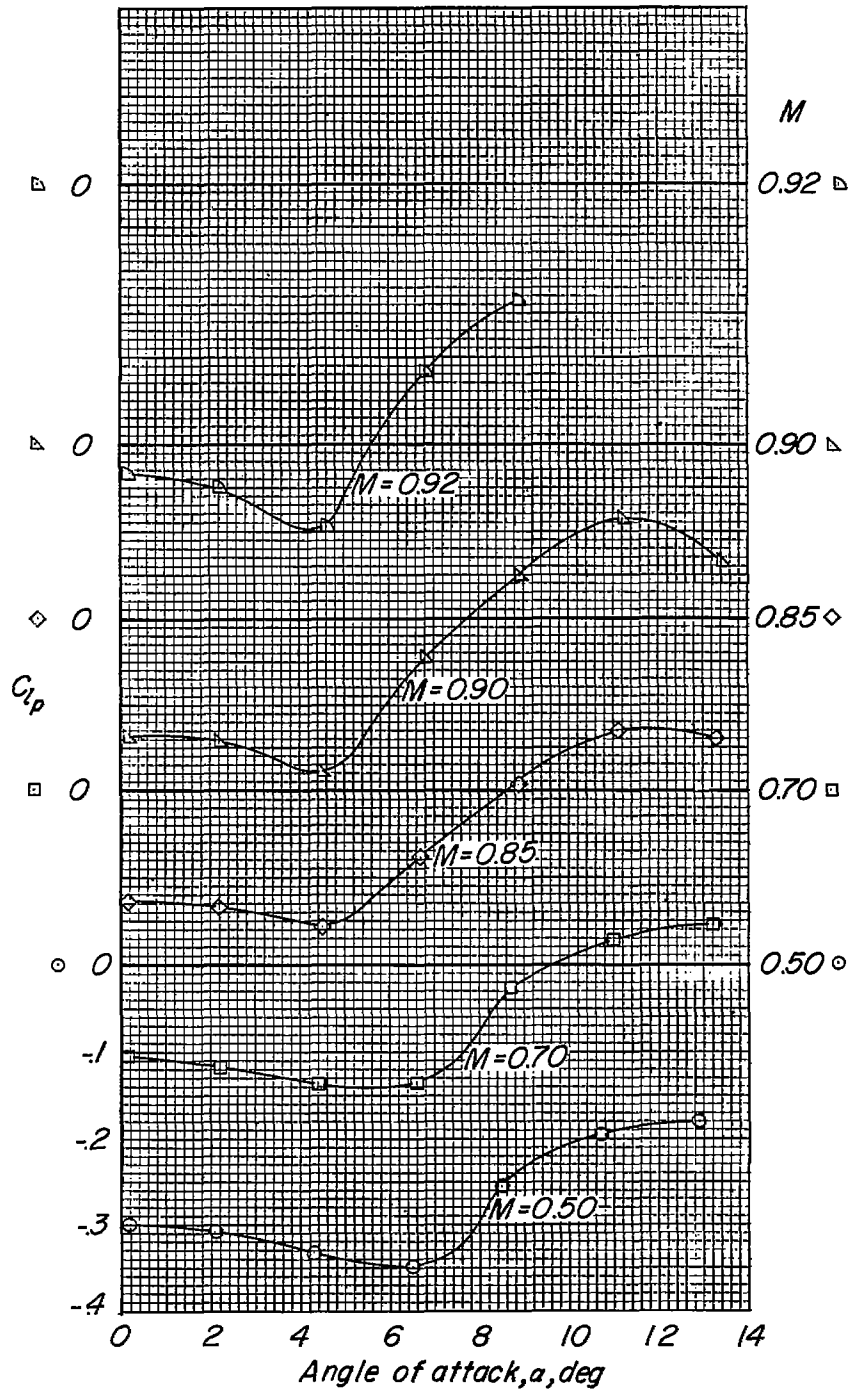

(a) Damping in roll C_{l_p}.

Figure 7.- Variation of rolling-stability derivatives with angle of attack for the aspect-ratio-4 wing swept back 45°.

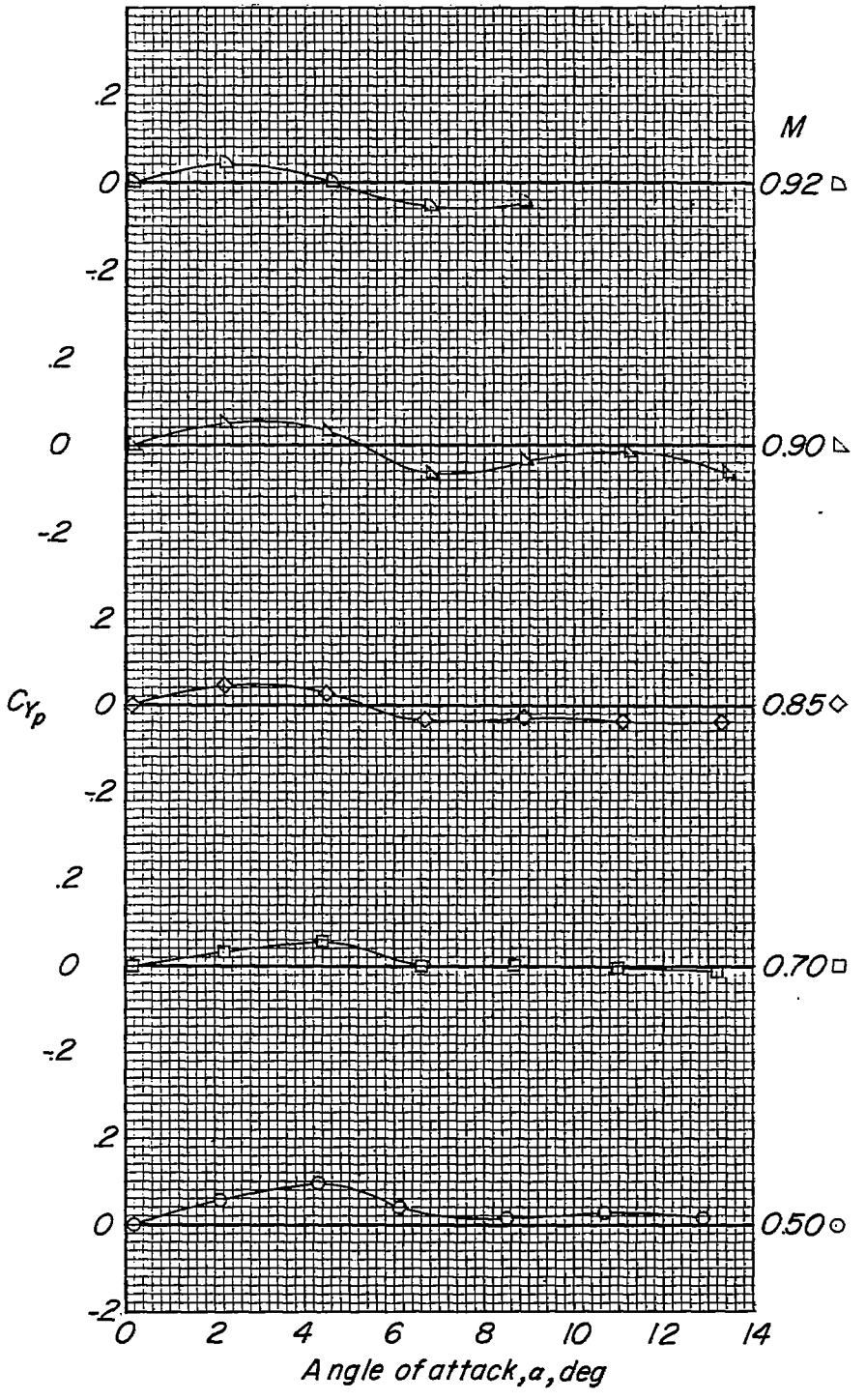

(b) Lateral force due to rolling C_{Y_p}.

Figure 7.- Continued.

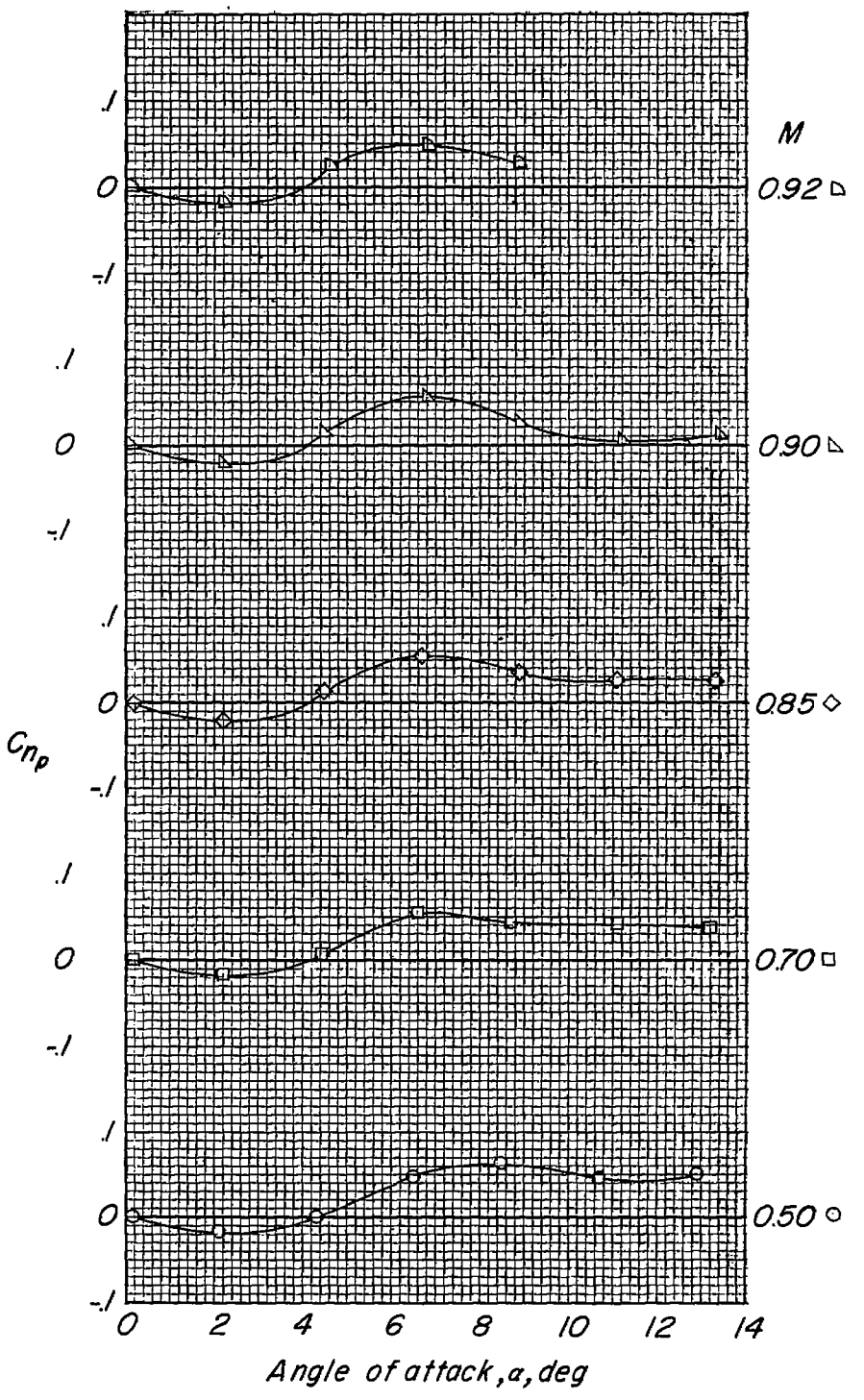

(c) Yawing moment due to rolling C_{n_p}.

Figure 7.- Concluded.

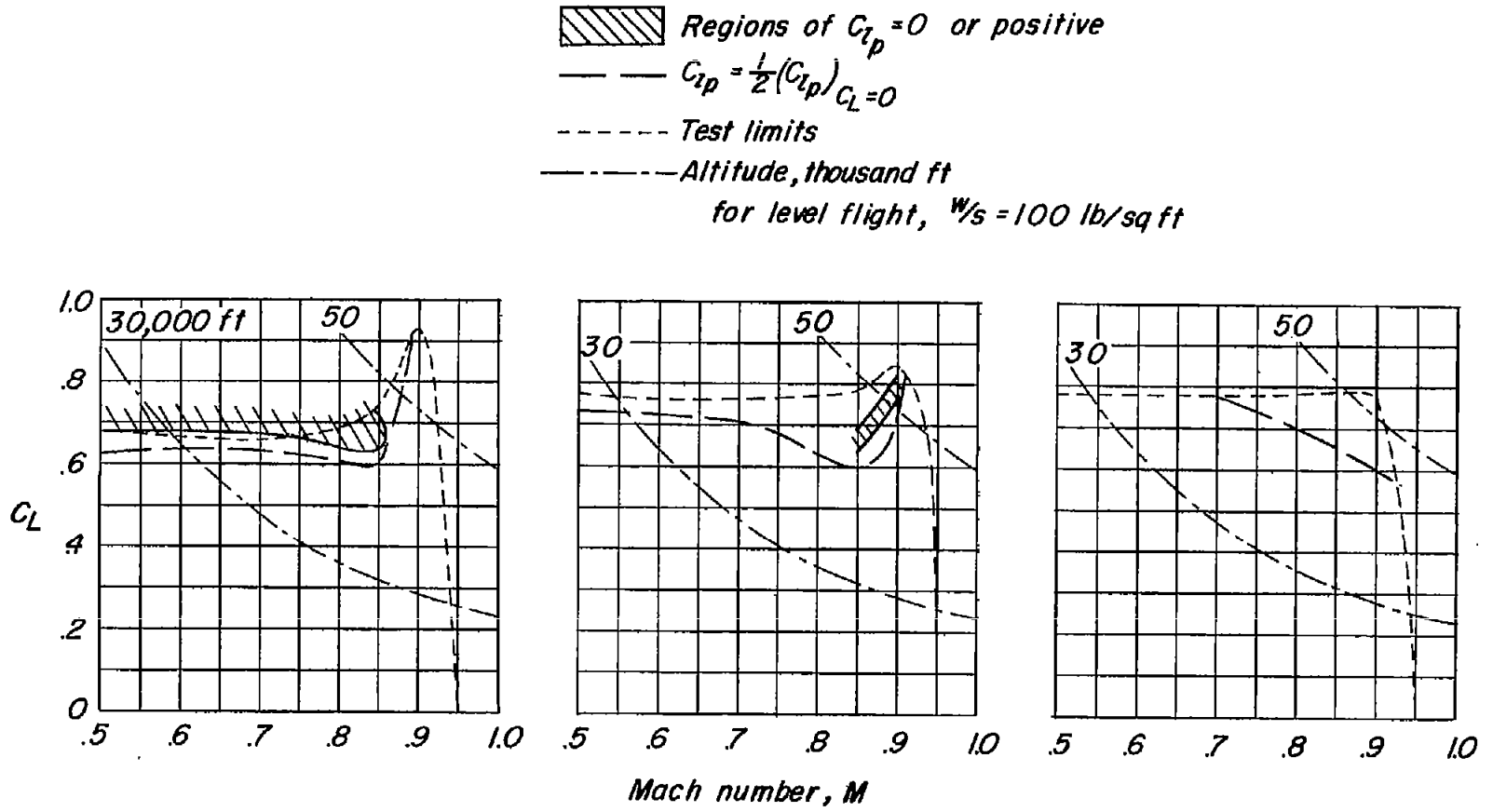

(a) Λ = 12.53; A = 3. (b) $\Lambda = 30^\circ$; A = 3. (c) $\Lambda = 45^\circ$; A = 4.

Figure 8.- Damping-in-roll boundaries for the test range of lift coefficient and Mach number.

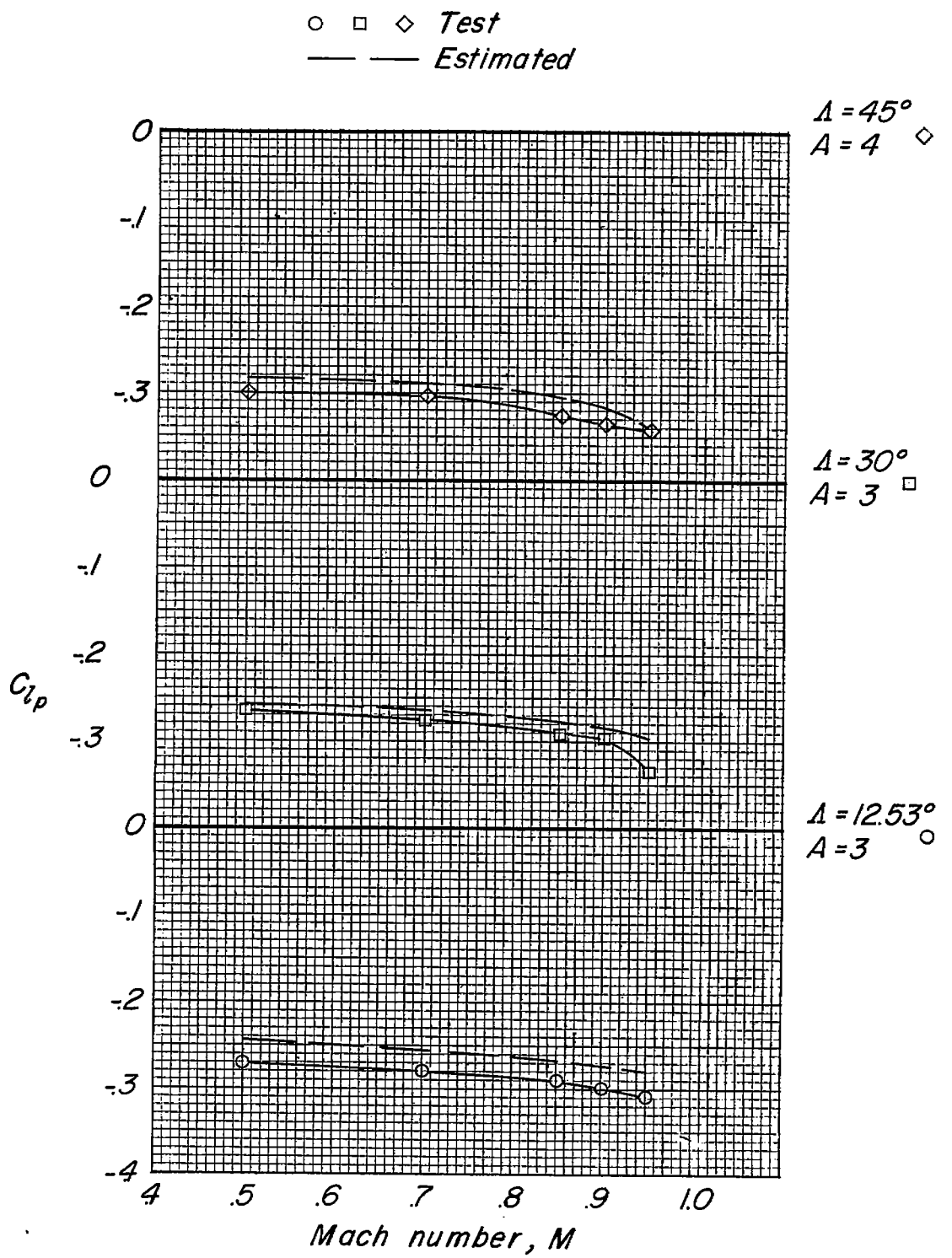

Figure 9.- Comparison of estimated and experimental variation of damping in roll at zero lift with Mach number.

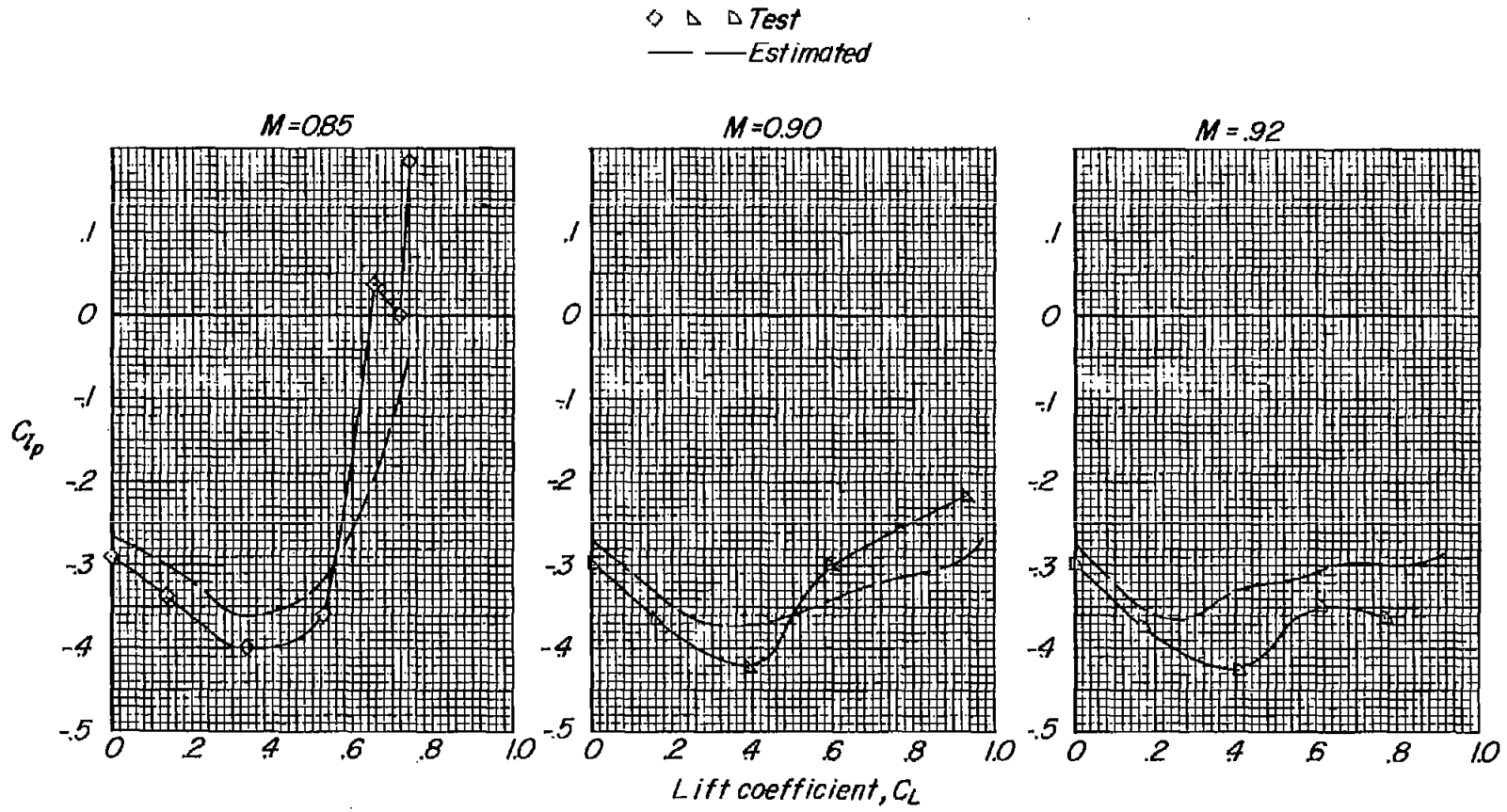

(a) $\Lambda = 12.53^{\circ}$; A = 3.

Figure 10.- Comparison of experimental and estimated variation of damping in roll with lift coefficient.

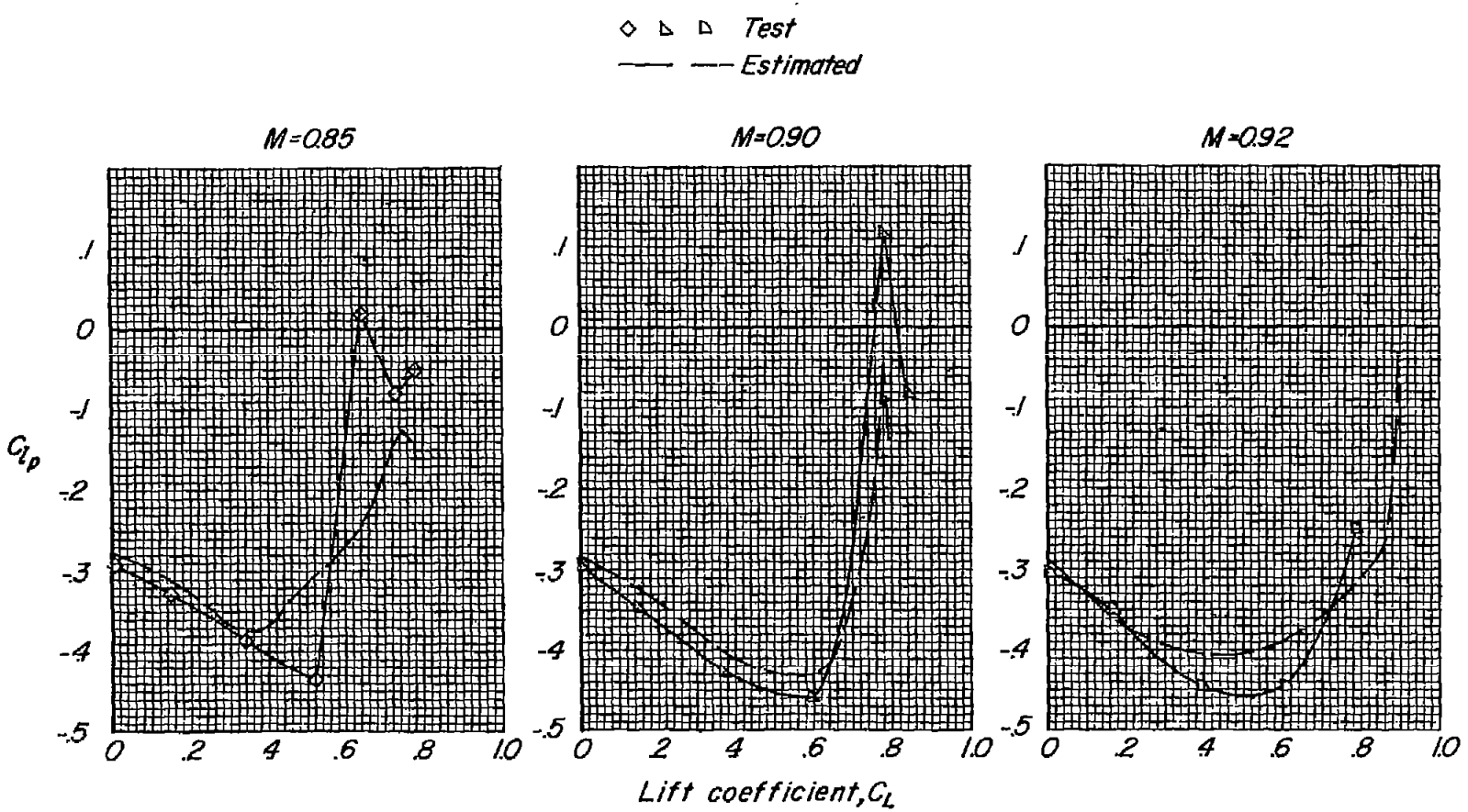

(b) $\Lambda = 30^{\circ}$; $A = 3$.

Figure 10.- Continued.

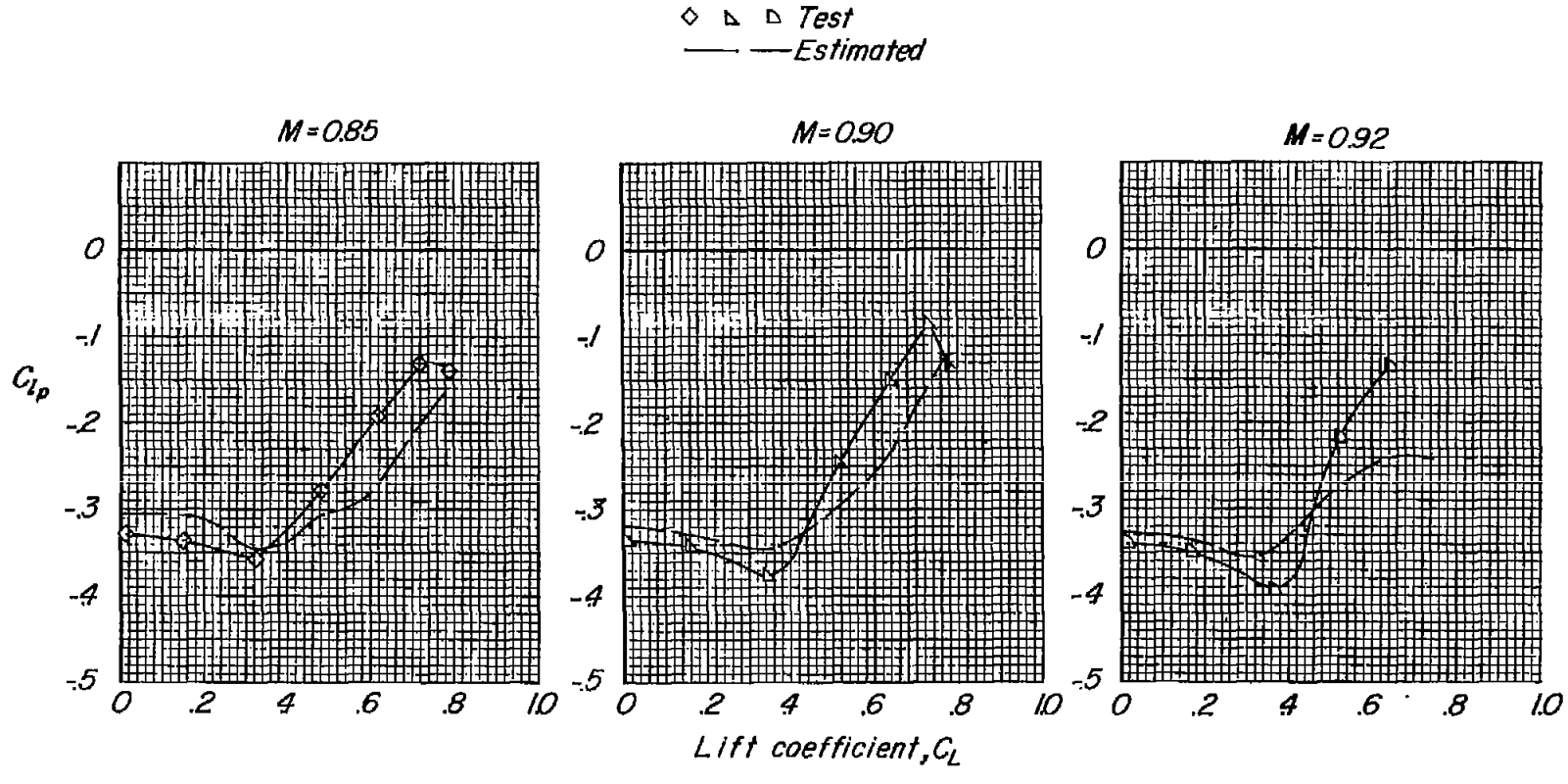

(c) $\Lambda = 45^\circ$; $A = 4$.

Figure 10.- Concluded.

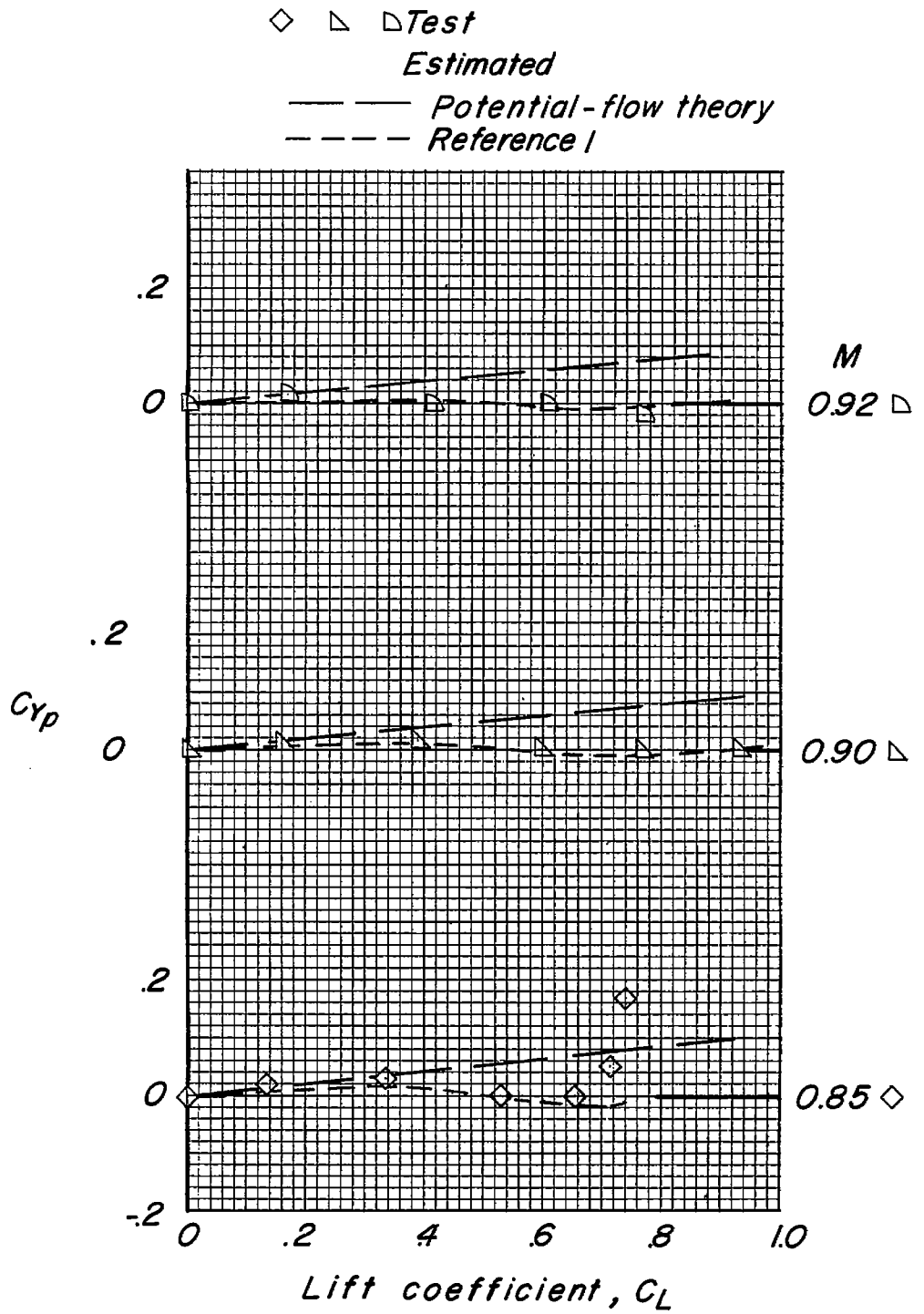

(a) $\Lambda = 12.53°$; $A = 3$.

Figure 11.- Comparison of experimental and estimated variation of lateral force due to rolling with lift coefficient.

[redacted]

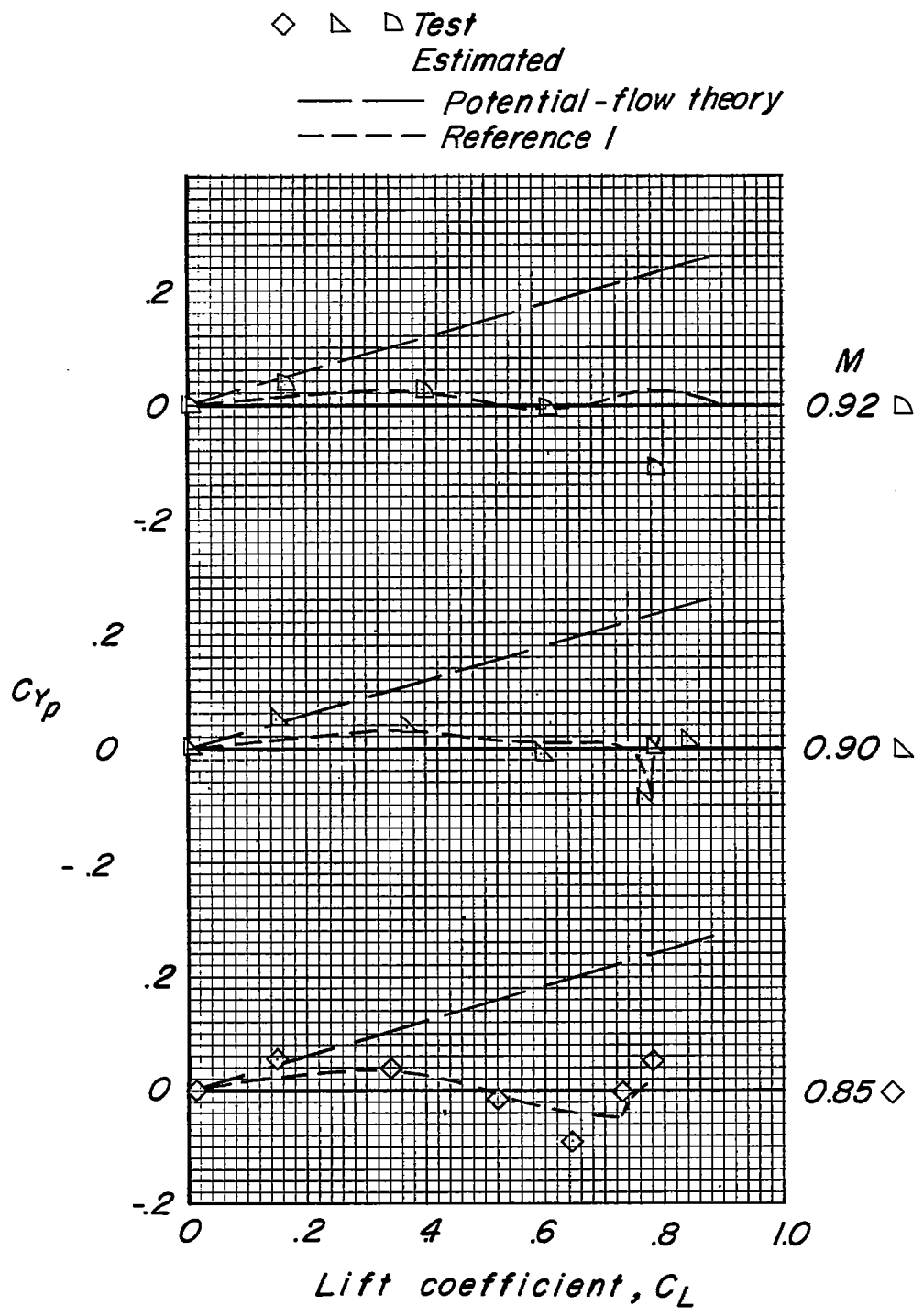

(b) $\Lambda = 30^\circ$; $A = 3$.

Figure 11.- Continued.

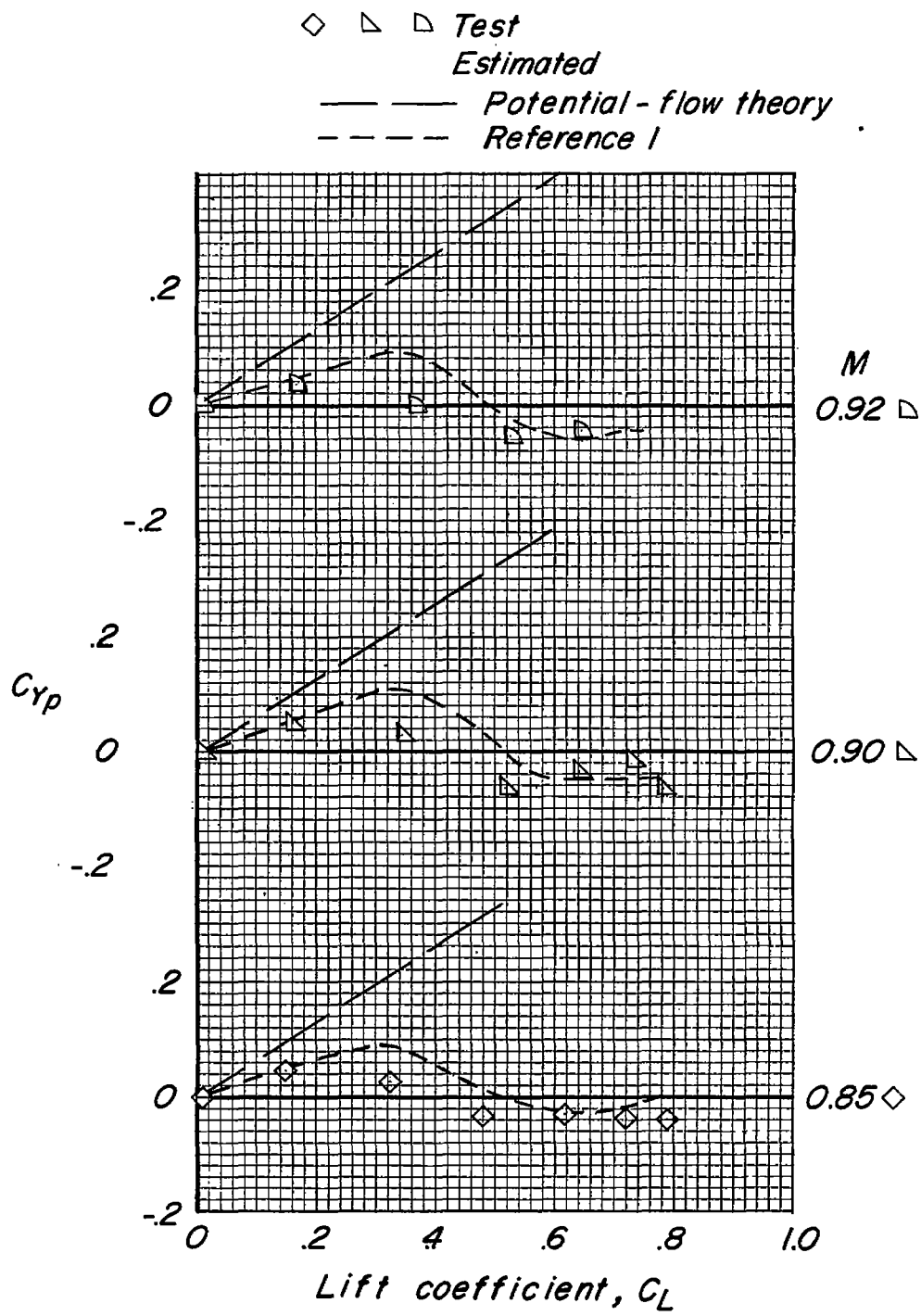

(c) $\Lambda = 45^\circ$; $A = 4$.

Figure 11.- Concluded.

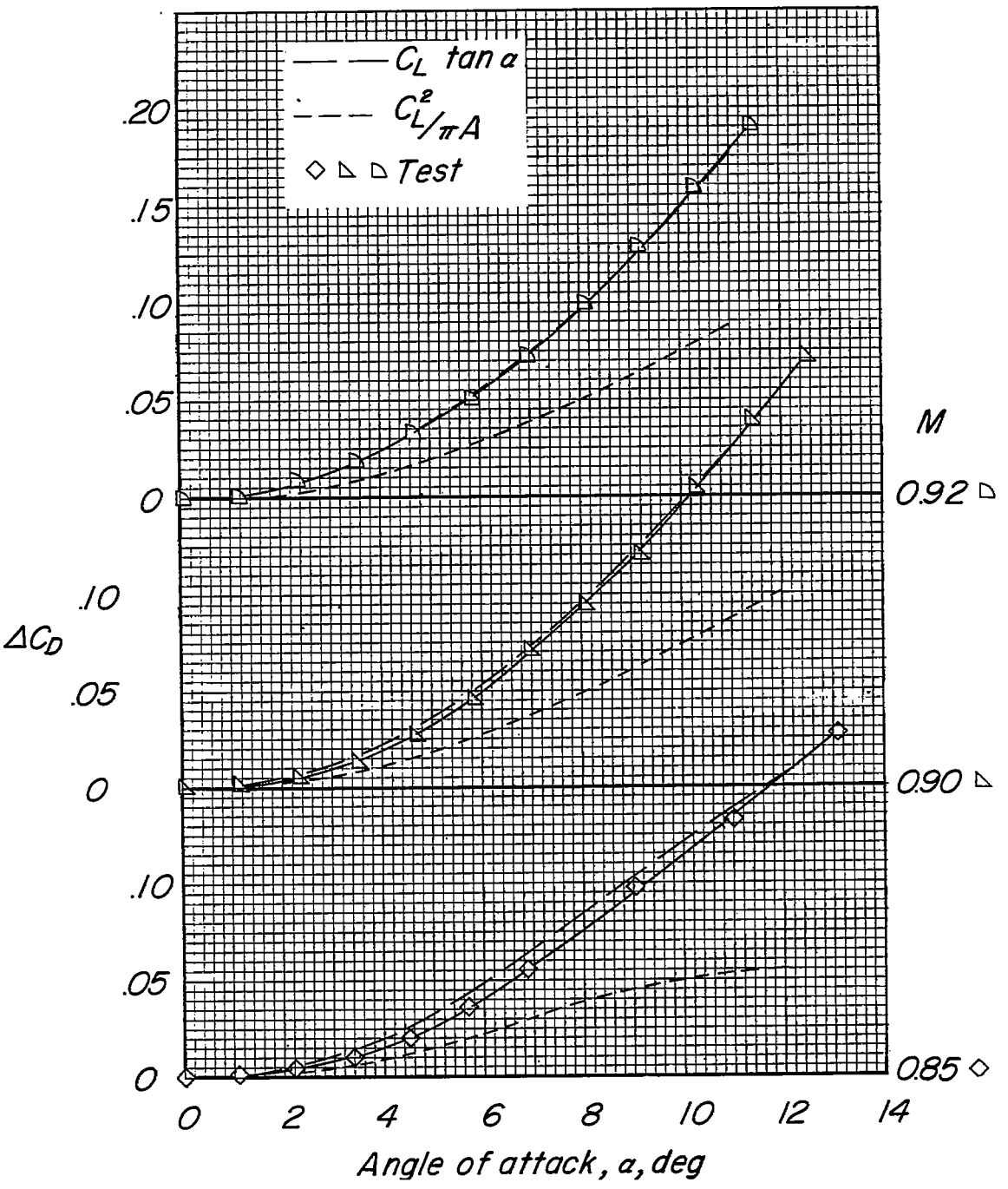

(a) $\Lambda = 12.53^\circ$; $A = 3$.

Figure 12.- Variation of drag due to lift with angle of attack.

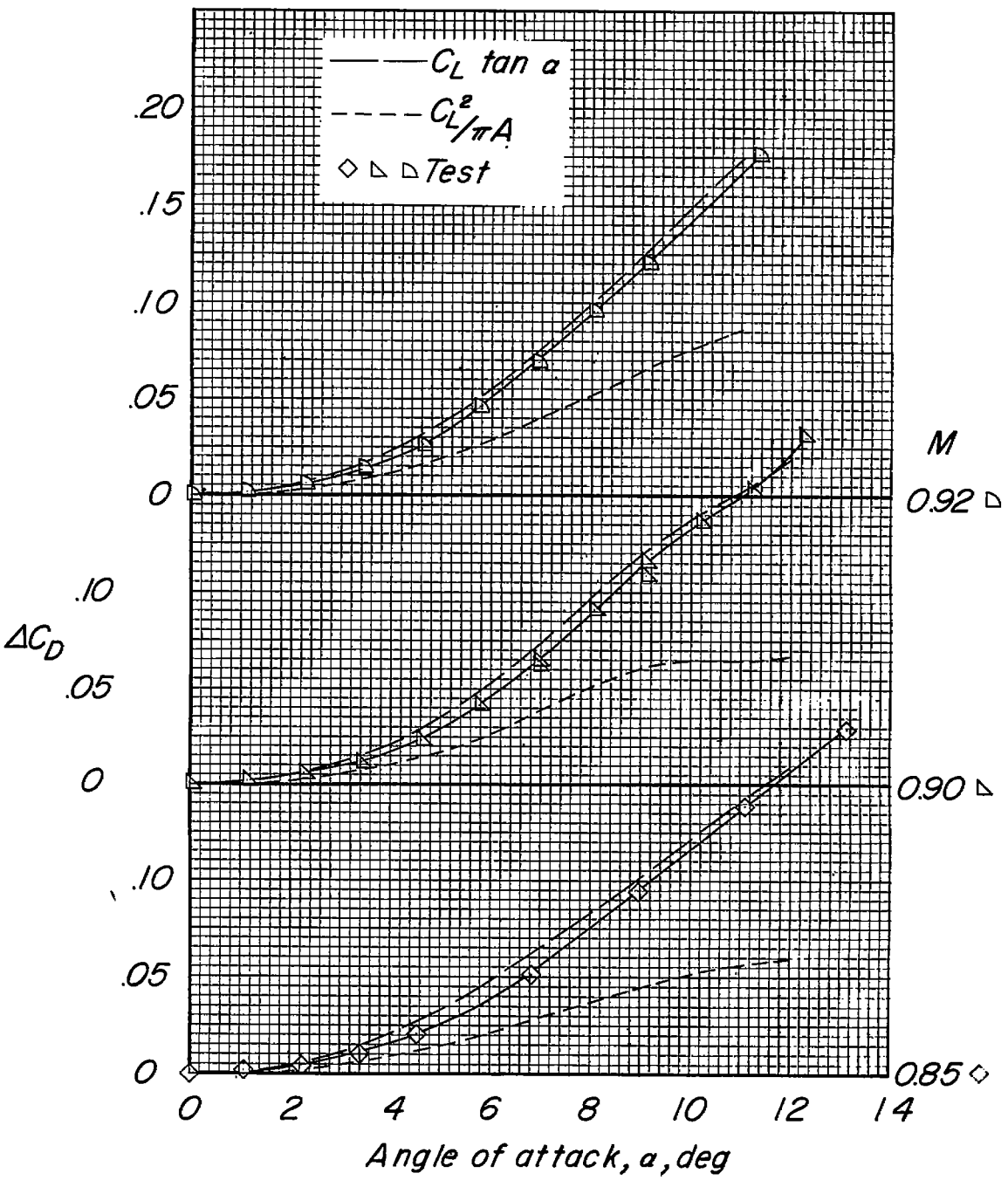

(b) $\Lambda = 30^\circ$; $A = 3$.

Figure 12.- Continued.

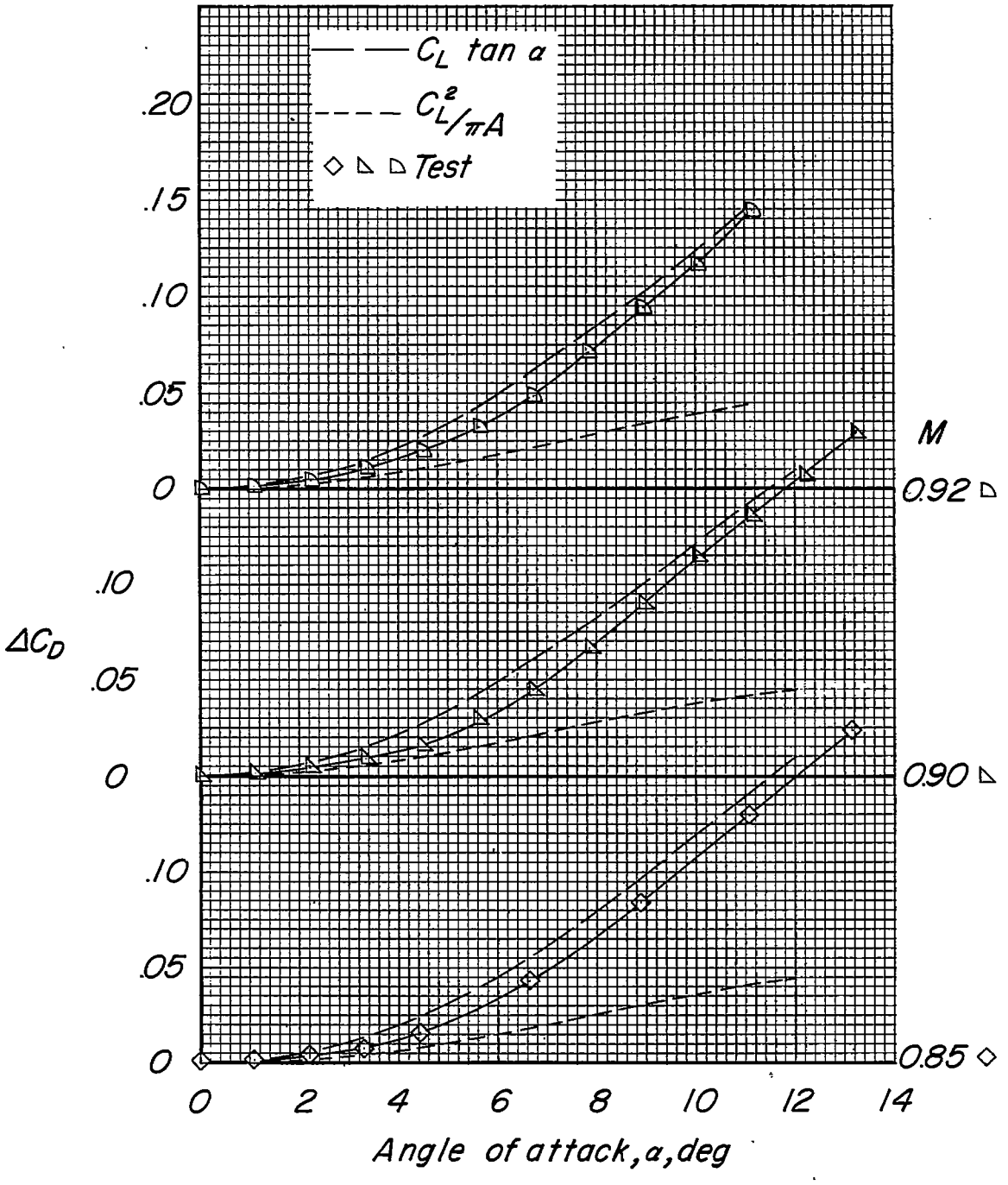

(c) $\Lambda = 45^\circ$; $A = 4$.

Figure 12.- Concluded.

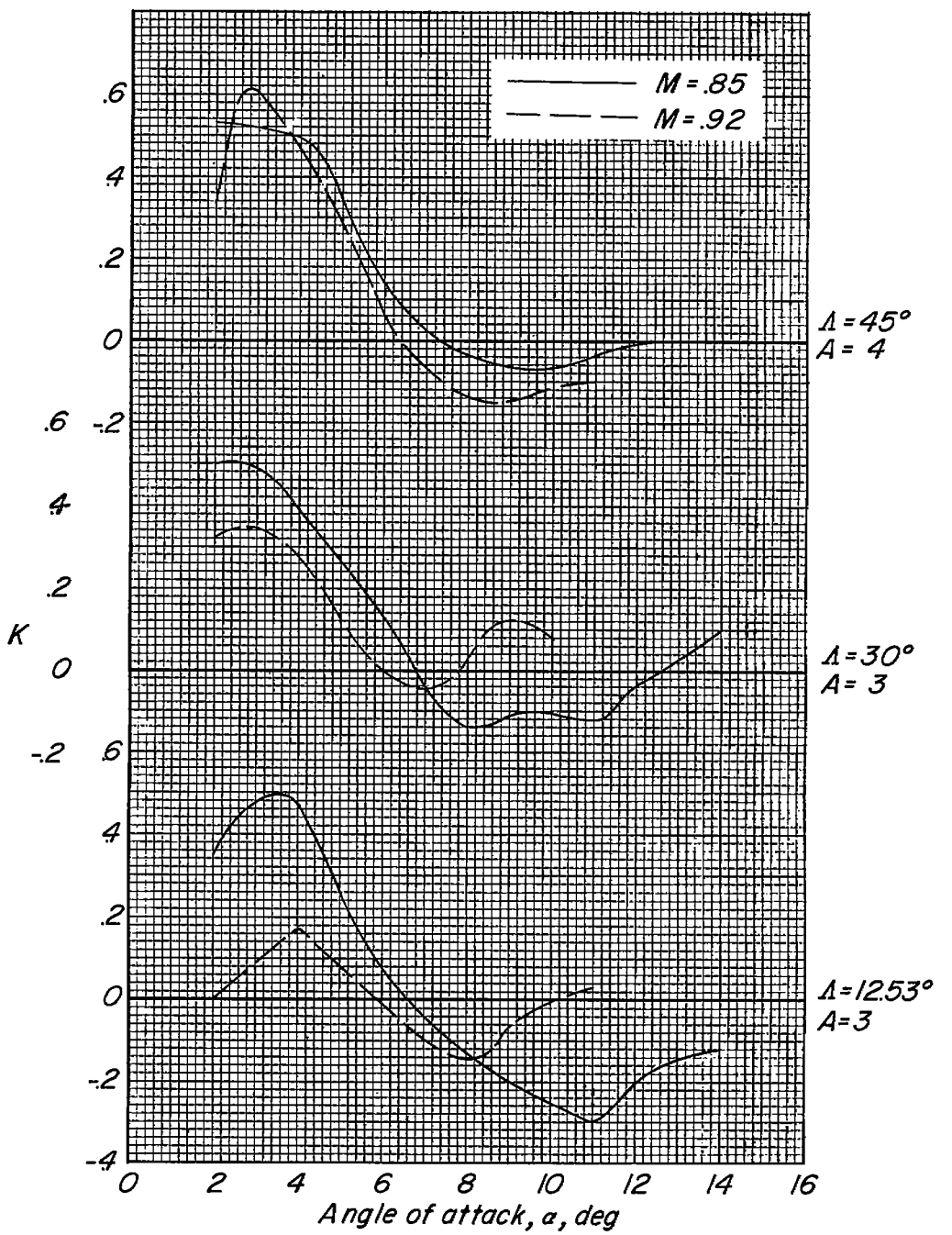

Figure 13.- Variation of the induced-drag factor K with angle of attack for the three test wings. $K = \dfrac{\dfrac{\partial(C_L \tan \alpha)}{\partial \alpha} - \dfrac{\partial(\Delta C_D)}{\partial \alpha}}{\dfrac{\partial(C_L \tan \alpha)}{\partial \alpha} - \dfrac{\partial(C_L^2/\pi A)}{\partial \alpha}}$

[redacted]

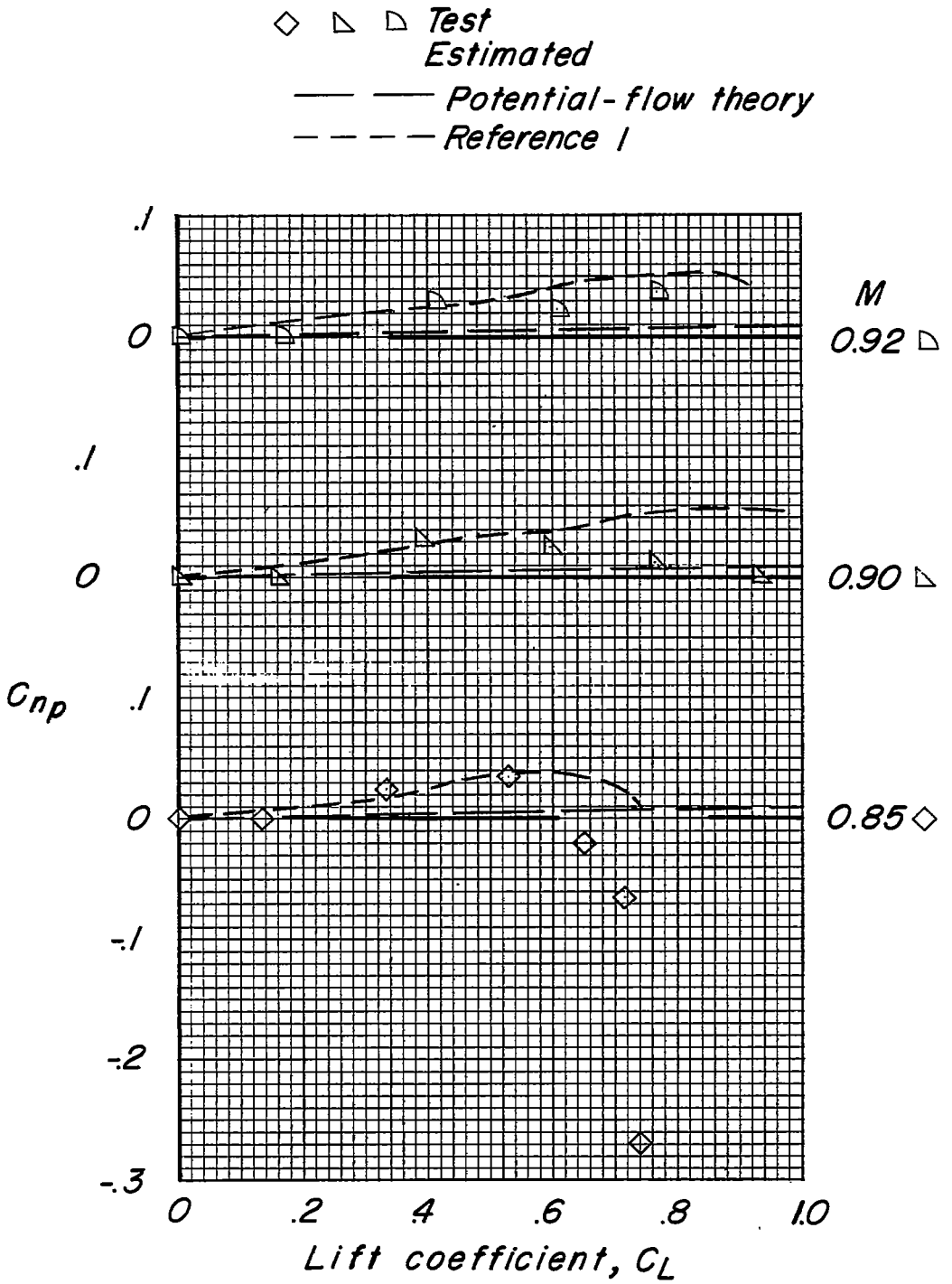

(a) $\Lambda = 12.53°$; $A = 3$.

Figure 14.- Comparison of experimental and estimated variation of yawing moment due to rolling with lift coefficient.

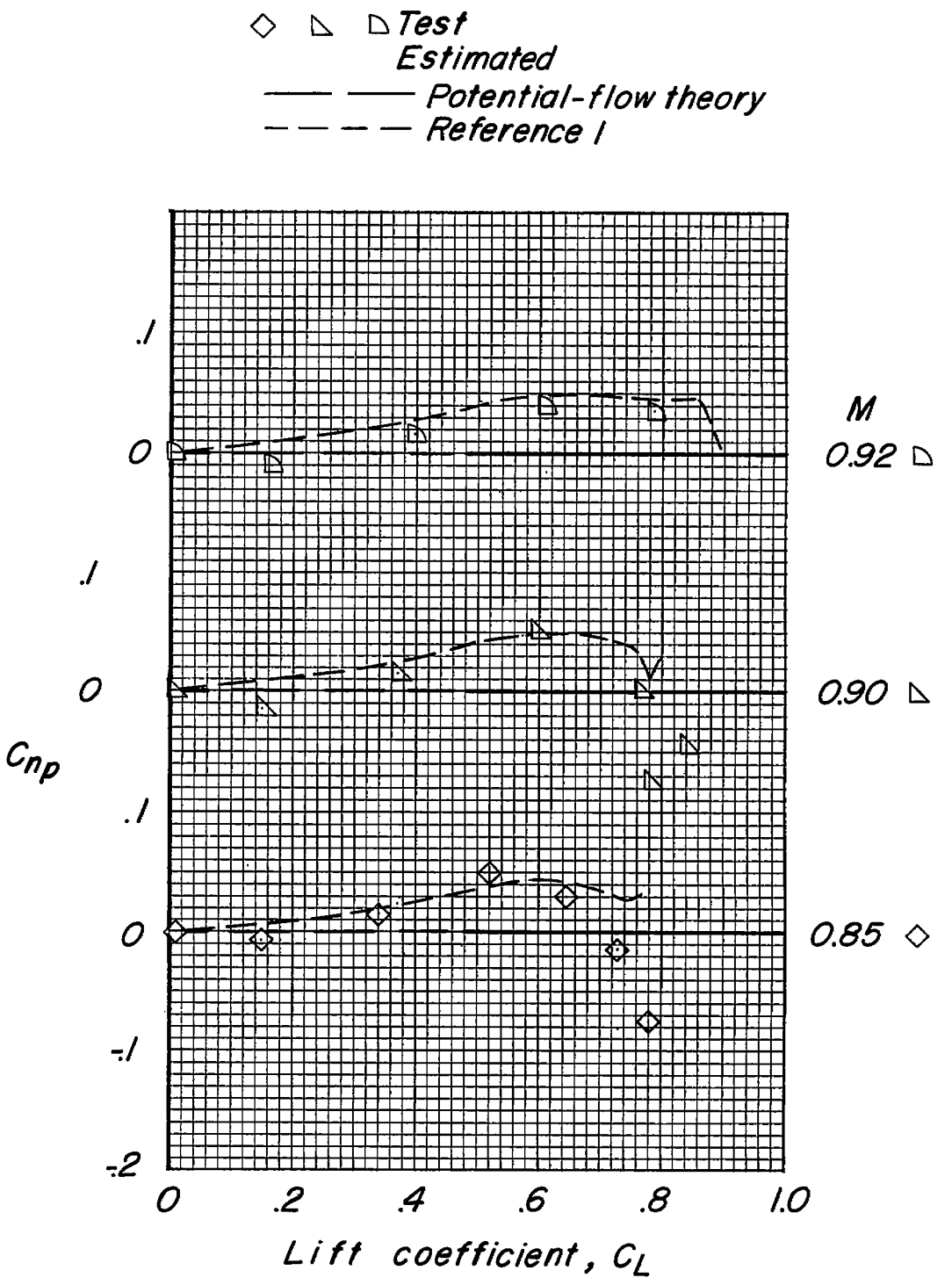

(b) $\Lambda = 30^\circ$; $A = 3$.

Figure 14.- Continued.

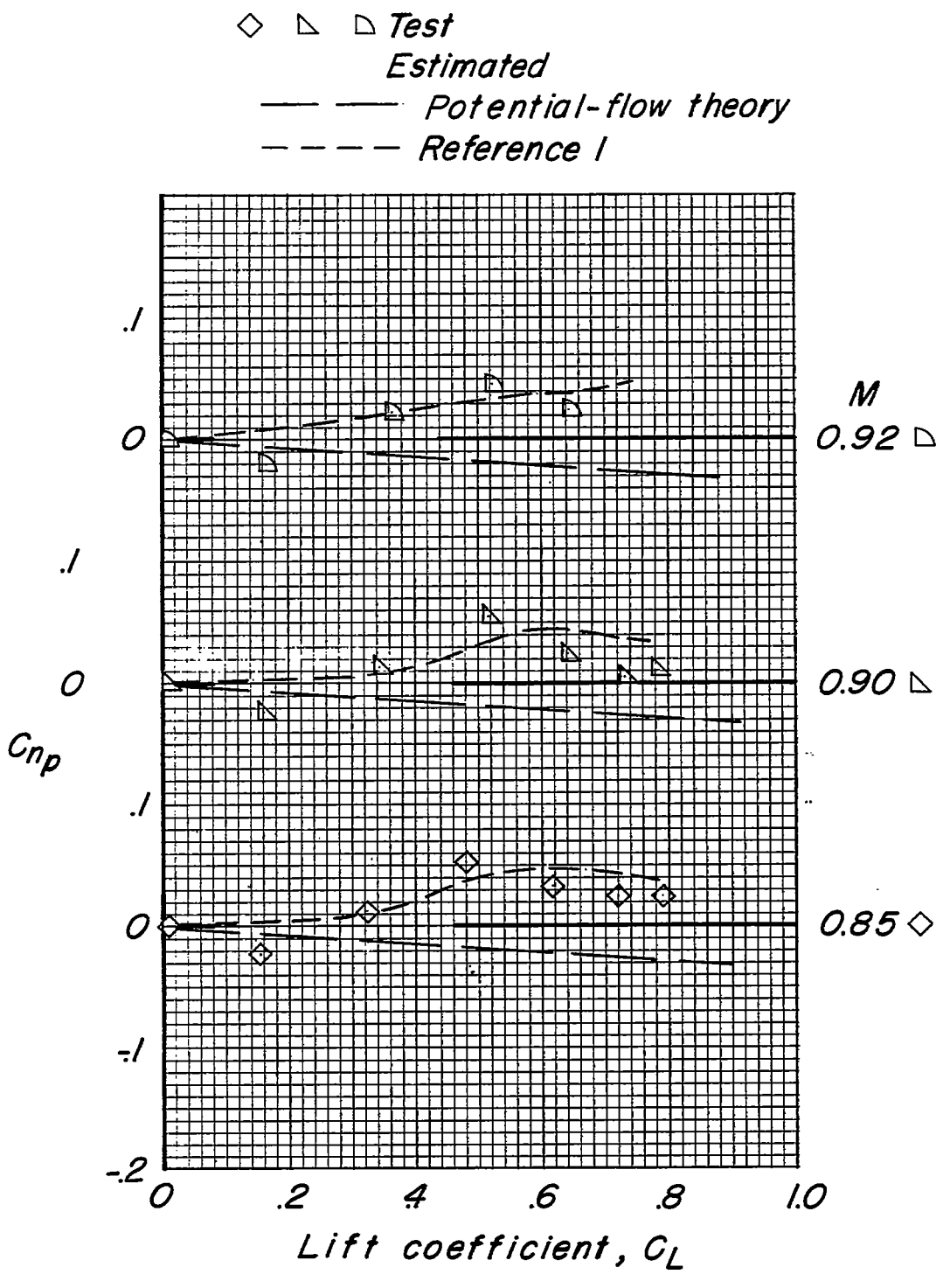

(c) $\Lambda = 45^\circ$; $A = 4$.

Figure 14.- Concluded.

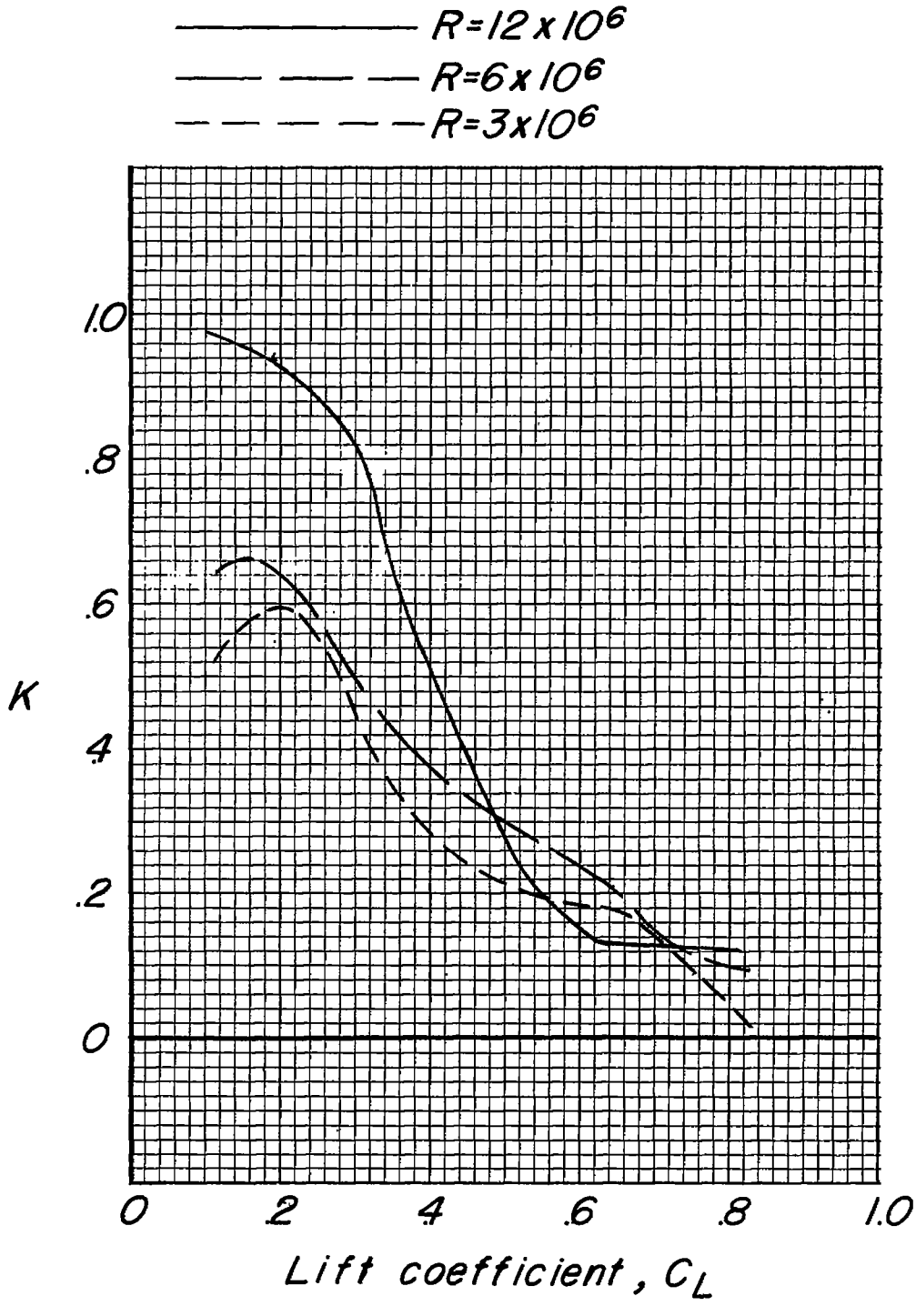

Figure 15.- Effect of Reynolds number on the variation of the factor K with lift coefficient as determined from low-speed tests of an aspect-ratio-4 wing swept back 45° and having a taper ratio of 0.30.

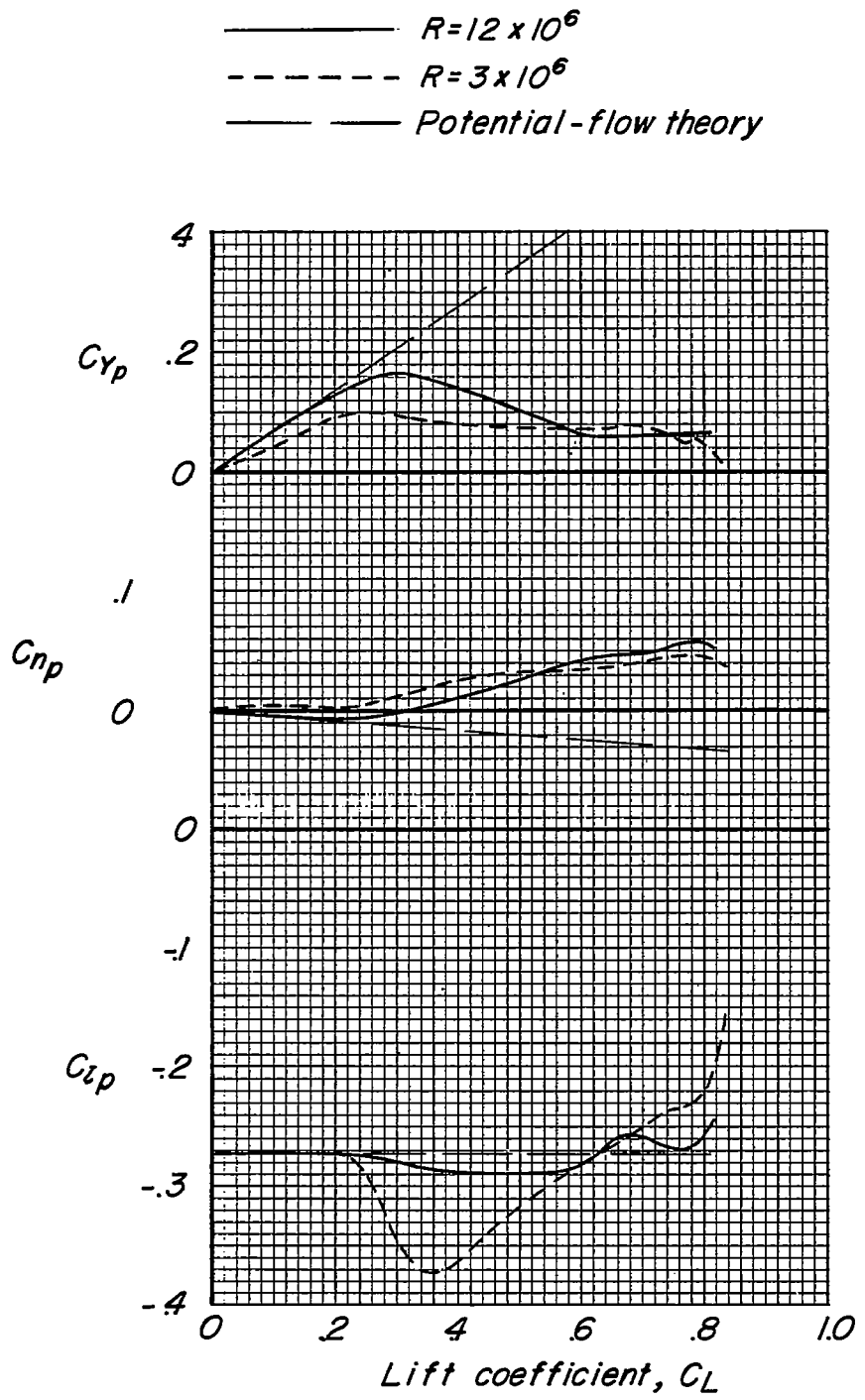

Figure 16.- Estimated effects of Reynolds number on the variation of rolling-stability derivatives with lift coefficient as determined from low-speed static-force data for an aspect-ratio-4 wing swept back 45° and having a taper ratio of 0.30.